Journal of Hazardous Materials 500 (2025) 140384

Contents lists available at ScienceDirect

Journal of Hazardous Materials

journal homepage: www.elsevier.com/locate/jhazmat

^{13}C metabolic tracing in human SGBS cells provides a potential new approach methodology for assessing metabolism-disrupting properties of environmental chemicals

Cornelius Goerdeler [a,1,2], Beatrice Engelmann [a,2,3], Helen Broghammer [b,4], Alix Sarah Aldehoff [a,5], Martin Wabitsch [c,d,6], Kristin Schubert [a,7], Matthias Blüher [b,d,e,8], John T. Heiker [b,9], Ulrike Rolle-Kampczyk [a,*,2,10], Martin von Bergen [a,d,f,g,2,11]

[a] Department of Molecular Toxicology, Helmholtz Centre for Environmental Research (UFZ), Leipzig, Germany
[b] Helmholtz Institute for Metabolic, Obesity and Vascular Research (HI-MAG) of the Helmholtz-Centre Munich at the University of Leipzig and University Hospital Leipzig, Leipzig, Germany
[c] Division of Pediatric Endocrinology and Diabetes, Ulm University Medical Center, Ulm, Germany
[d] German Centre for Child and Adolescent Health (DZKJ), Germany
[e] Department of Endocrinology, Nephrology and Rheumatology, University of Leipzig, Leipzig, Germany
[f] Institute of Biochemistry, Leipzig University, Leipzig, Germany
[g] German Centre for Integrative Biodiversity Research (iDiv) Halle-Jena-Leipzig, Leipzig, Germany

HIGHLIGHTS

- ^{13}C tracing in SGBS adipocytes enables sensitive detection of metabolic alterations
- MINCH acts mainly at μM levels but has slight effects in preadipocytes at nM levels
- MINCH rewired metabolism towards lipid synthesis in human preadipocytes
- MINCH induced browning in mature human adipocytes
- Effects resembled PPARγ agonist rosiglitazone but appeared partly PPARγ-independent

GRAPHICAL ABSTRACT

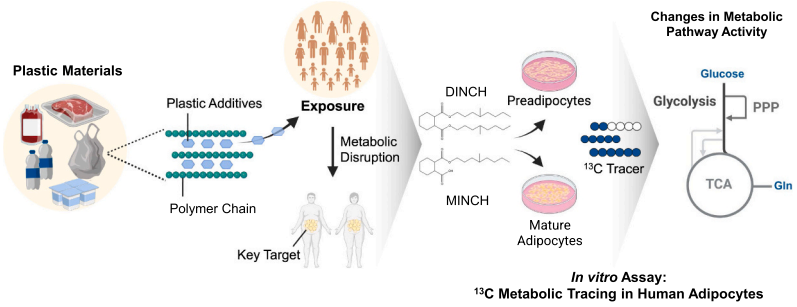

* Correspondence to:Department of Molecular Toxicology. Helmholtz Center for Environmental Research, Permoserstraße 15, Leipzig 04318, Germany.
E-mail address: ulrike.rolle-kampczyk@ufz.de (U. Rolle-Kampczyk).
[1] https://orcid.org/0000-0002-6422-4738
[2] Authors contributed equally
[3] https://orcid.org/0000-0002-8807-9651
[4] https://orcid.org/0009-0004-9954-1938
[5] https://orcid.org/0000-0001-7994-5725
[6] https://orcid.org/0000-0001-6795-8430
[7] https://orcid.org/0000-0003-4365-084X
[8] https://orcid.org/0000-0003-0208-2065
[9] https://orcid.org/0000-0003-2822-3006
[10] https://orcid.org/0000-0002-7728-6284
[11] https://orcid.org/0000-0003-2732-2977

https://doi.org/10.1016/j.jhazmat.2025.140384
Received 3 July 2025; Received in revised form 19 October 2025; Accepted 3 November 2025
Available online 4 November 2025

ARTICLE INFO

Keywords:
Plasticizer
DINCH
New Approach Methodology
Metabolic disruption
^{13}C metabolic tracing

ABSTRACT

Human exposure to certain environmental chemicals, including phthalates, is linked to metabolic disruption and may thereby contribute to diseases like obesity. However, regulatory methods to evaluate such effects are lacking. DINCH was introduced as a substitute for banned phthalate plasticizers, but its primary metabolite, MINCH, has been shown to promote adipogenesis in human preadipocytes and alter the lipid metabolism of mature adipocytes. To investigate its potential metabolism-disrupting effects, we assessed changes in the central carbon metabolism activity of human preadipocytes and mature adipocytes by ^{13}C metabolic tracing. In preadipocytes, MINCH increased glycolysis, pentose phosphate pathway activity, acetyl-CoA production from glucose and glutamine, and pyruvate anaplerosis, indicating a metabolic shift toward adipogenesis. In mature adipocytes, MINCH enhanced glycolysis, glyceroneogenesis, fatty acid oxidation, and oxidative TCA cycle activity, pathways associated with the browning of adipocytes. Elevated UCP1 expression confirmed MINCH-induced browning. Most pronounced effects occurred at micromolar concentrations, whereas subtle changes were already observed at nanomolar concentrations in preadipocytes, the biological relevance of which should be further investigated. Overall, our findings demonstrate the utility of ^{13}C metabolic tracing as a New Approach Methodology for detecting chemical-induced metabolic alterations, thus providing a new perspective for the hazard and risk assessment of environmental contaminants.

1. Introduction

Between 1990 and 2022, the global age-standardized prevalence of obesity more than doubled in adult women and men [1]. This increase in prevalence rates is associated with a rise in serious illnesses and a high-cost burden for the public health system [2], as obesity is a key cause of several comorbidities, including type 2 diabetes (T2D) and fatty liver disease [3,4]. While genetics play a significant role in the pathogenesis of obesity, with heritability reaching up to 70 % in twin studies [5,6], lifestyle factors such as reduced physical activity [7] and increased consumption of energy-dense, ultra-processed food [8,9] also contribute. Besides genetic factors, emerging evidence suggests that exposure to certain environmental chemicals might further promote obesity or metabolic diseases [10–12]. Mechanistically, these chemicals primarily act by interfering with the endocrine system, thereby disrupting central metabolic processes and leading to the development of metabolic diseases [13]. Hence, they are referred to as metabolism-disrupting chemicals (MDCs) [13]. White adipose tissue (WAT) is a key target for MDCs as it is essential for maintaining energy homeostasis through lipid storage and release, and as an endocrine organ through the secretion of adipokines such as leptin, involved in the regulation of hunger and satiety [14,15]. MDCs may alter white adipose tissue function by promoting adipocyte differentiation [16,17], modulating the number and size of adipocytes [18], inducing a dysfunctional adipocyte state with impaired insulin sensitivity [19], altering adipokine secretion profiles [17,20], as well as changing the ratio of visceral to subcutaneous adipose tissue [21]. Apart from the effects on WAT, MDCs have also been shown to affect thermogenic fat depots such as brown adipose tissue (BAT) and brite adipocytes, which are white adipocytes that acquire brown-like characteristics through a process known as browning [22,23]. Both brown and brite adipocytes express uncoupling protein 1 (UCP1), which mediates non-shivering thermogenesis and is therefore important for whole-body energy expenditure [22]. MDCs may suppress thermogenic activity by reducing UCP1 expression or promoting the whitening of BAT [24,25], and conversely, enhance thermogenic activity by increasing UCP1 expression in BAT [26] or inducing the browning of WAT i.e., the formation of brite adipocytes [27].

The rise in global plastic production and the ubiquitous presence of plastic materials have increased human exposure to plastic additives [28,29], particularly to phthalates, which dominate the global plasticizer consumption [30]. Several studies suggest that certain phthalates, such as DEHP, have obesogenic properties [10,31], and elevated human exposure is positively associated with measures of obesity [32]. The primary metabolite of DEHP, MEHP, induced adipogenesis in murine and human adipocytes [33,34] and increased fat mass, altered serum adipokine and lipid levels [35–37], induced adipocyte hypertrophy [37], and impaired insulin sensitivity [35] in mice *in vivo*.

Following the restriction of DEHP and other phthalates in the EU and the US [38,39], there has been a shift towards the use of replacement products [40]. The cyclohexanoate plasticizer DINCH was introduced for use in sensitive applications and food contact materials [41]. Nonetheless, *in vitro* studies have shown that MINCH, the primary metabolite of DINCH, induces adipogenesis in rat and human preadipocytes and alters adipokine secretion and lipid metabolism of mature human adipocytes [42,43]. Similar to MEHP [33,36,44], these effects appear to be mainly mediated by activation of the nuclear hormone receptor peroxisome proliferator-activated receptor gamma (PPARγ) [42,45,46], one of the master regulators of adipogenesis. However, application studies performed according to OECD guidelines did not reveal any obesogenic effect of DINCH in Wistar rats [47]. In line, dietary DINCH-exposed C57BL/6 N mice showed no increase in weight gain or changes in body composition, but an increase in adipocyte size in visceral adipose tissue and significant sex-specific effects on serum lipid levels with impaired insulin sensitivity, and alterations in protein levels of serum, liver, and adipose tissue related to energy metabolism [48]. Given these results and the limited number of studies, the metabolism-disrupting properties of DINCH warrant further investigation.

As the internationally applied OECD guidelines for testing chemicals are currently not specifically designed for assessing metabolism-disrupting properties, there is a need for the development of new assessment strategies to analyze DINCH and other emerging chemicals [49]. To reduce traditional animal-based methods, New Approach Methodologies (NAMs) such as omics-based techniques and *in vitro* testing systems should be prioritized [49,50]. Apart from transcriptomics [51] and proteomics [52], metabolomics is emerging as a sensitive method for studying metabolism-disrupting properties of chemicals [53–55], especially as changes in metabolites are highly reflective of phenotypic changes [56].

We recently used metabolomics in human SGBS cells to analyze the effects of DINCH and MINCH on preadipocytes [57]. However, our method has so far relied on measuring changes in metabolite levels, which do not necessarily relate to changes in pathway activity. To overcome this limitation, we applied ^{13}C metabolic tracing to infer the pathway activity of the central carbon metabolism in human adipocytes upon chemical exposure. DINCH and MINCH exposure was performed in preadipocytes to analyze effects on adipogenesis and in mature adipocytes to assess effects on differentiated adipocytes.

Changes in pathway activity of the central carbon metabolism were analyzed after incubation for 3 and 24 h with three carbon tracers. [U-^{13}C]glucose tracer was selected to analyze glycolysis and pentose

phosphate pathway (PPP) activity, glucose contribution to the tricarboxylic acid (TCA) cycle, and pyruvate carboxylase-mediated anaplerosis [58]. [U-^{13}C]glutamine assessed glyceroneogenesis activity, the glutamine contribution to the TCA cycle, the oxidative flow through the TCA, the reductive carboxylation via isocitrate dehydrogenase (IDH) for lipid synthesis, and the cycling of metabolites through the TCA cycle [58,59]. [1,2-^{13}C]glucose labeling validated glycolysis and PPP activity and distinguished their contribution to glucose metabolism (i.e., glycolysis and PPP) through PPP-associated carbon loss [58,60].

2. Materials and methods

The plasticizer diisononyl-cyclohexane-1,2-dicarboxylate (DINCH) was purchased from abcr (CAS no. 166412–78–8, Cat. No. AB440048, 98 % purity; Karlsruhe, Germany). Mono-isononyl-cyclohexane-1,2-dicarboxylate (MINCH), cyclohexane-1,2-dicarboxylic acid mono-carboxyisooctyl ester (cx-MINCH), cyclohexane-1,2-dicarboxylic acid mono(hydroxy-isononyl) ester (OH-MINCH), and cyclohexane-1,2-dicarboxylic acid mono(oxo-isononyl) ester (oxo-MINCH) were obtained from Toronto Research Chemicals (Cat.No. C987305, 95 % purity; C987315, 96 % purity; H949710, 98 % purity; and M329200, 97 % purity; Toronto, ON, Canada). Synthesis information and the exact isomer composition of DINCH were not disclosed by the manufacturer. For all cell culture experiments, the 4-methyloctyl isomer of MINCH was used. Phthalic acid mono-2-ethylhexyl ester (MEHP), purchased from Sigma Aldrich (Nürmbrecht, Germany), was used as an internal standard for MS measurement of DINCH and its metabolites. The cell culture medium for all adipocyte cultivation was DMEM/F12 cell medium (1:1) (Cat.No. 11320033; Thermo Fisher Scientific, Waltham, MA, USA). The customized medium (Thermo Fisher Scientific, Waltham, MA, USA) for the stable isotopic labeling experiment did not contain glucose, pyruvate, glutamine, glutamate, alanine, serine, glycine, and aspartate. [U-^{13}C]glucose (99 %) and [1,2-^{13}C]glucose (99 %) were purchased from Sigma Aldrich (99 %, St. Louis, MO, USA) and [U-^{13}C]glutamine (99 %) from Cambridge Isotope Laboratories (Tewksbury, MA, USA).

2.1. Cell cultivation and labeling experiment

The human Simpson-Golabi-Behmel syndrome (SGBS) preadipocyte cell strain, which were derived from the subcutaneous adipose tissue of a male human infant with SGBS, was used as a human adipocyte model system [61]. The SGBS cells were provided by Prof. Martin Wabitsch's laboratory at the University Hospital Ulm and cultivated in 0 F medium (containing 33 µM biotin, 17 µM pantothenate, 100 µg/mL streptomycin, and 100 IU/mL penicillin) with 10 % FCS (Gibco, Carlsbad, CA, USA) at 37 °C and 5 % CO_2 in 95 % humidity. Cultivation was carried out in cell culture products from TPP (Trasadingen, Switzerland) and Sarstedt (Nümbrecht, Germany). Both companies declared their cell culture products 'plasticizer-free'.

SGBS adipocytes were maintained and differentiated according to the standard protocol described previously [61]. Briefly, SGBS preadipocytes were grown to confluence and differentiated by adding QuickDiff medium (serum-free 0 F medium supplemented with 2 µM rosiglitazone, 25 nmol/L dexamethasone, 0.5 mmol/L 3-isobutyl-1-methylxanthine, 0.1 µmol/L cortisol, 0.01 mg/mL transferrin, 0.2 nmol/L triiodothyronine, and 20 nmol/L human insulin). After 4 days, the medium was exchanged with 3FC medium (serum-free 0 F medium supplemented with 0.1 µmol/L cortisol, 0.01 mg/mL transferrin, 0.2 nmol/L triiodothyronine, and 20 nmol/L human insulin).

To assess the effects of MINCH on adipogenesis, preadipocytes were cultivated in 12-well plates and treated for 12 days with differentiation media without the PPARγ agonist rosiglitazone, supplemented with 10 nM and 10 µM MINCH (Figure S1A). The lower dose of 10 nM MINCH was selected as it corresponds to the concentrations of metabolites of phthalate plasticizers found in human serum [62] and values for DINCH metabolites in human serum are missing so far. The higher concentration was selected to consider a high exposure scenario, e.g., after medical treatment, as it has been shown for the phthalate plasticizer DEHP that blood levels up to 100–1000 times higher than in the general population can occur [63]. Effects of DINCH on adipogenesis were not assessed because no effects on the metabolism of treated SGBS preadipocytes were observed, as previously described [57]. To obtain a positive differentiation control, SGBS cells were exposed to rosiglitazone. The effects were compared to untreated control SGBS cells. To control for the effects of the vehicle solvent, MeOH and DMSO were added to a final concentration of 0.01 % (v/v) and 0.02 % (v/v), respectively, to all cell culture media. The cell culture medium was exchanged every second day for continuous exposure simulation.

For studying the effects on mature adipocytes, all cells were differentiated according to the standard protocol until day 12 (Figure S1B) [61]. Cells were treated with 10 nM and 10 µM MINCH, as well as 10 µM DINCH, until day 20, alongside the control of rosiglitazone exposure and the untreated control. Although DINCH solubility is limited and no effects on preadipocyte metabolism were observed [57], effects of DINCH on the metabolism of mature adipocytes were analyzed, as previous proteome analysis indicated changes following 10 nM DINCH treatment of SGBS cells [42].

For isotopic labeling experiments, treated cells were first insulin-starved 16 h before day 12 or day 20, respectively. Subsequently, the medium was replaced with 3FC medium prepared with customized DMEM/F12 in which either glucose or glutamine was replaced with the respective stable isotope-labeled analog [1,2-^{13}C]glucose, [U-^{13}C]glucose or [U-^{13}C]glutamine, respectively, and conditioned according to the treatment (DINCH, MINCH rosiglitazone or control). All labeling media were supplemented with insulin (20 nM) to stimulate glucose uptake and lipid synthesis, thereby promoting metabolic activation [64]. This approach was chosen to enhance ^{13}C tracer incorporation and facilitate the detection of treatment-induced changes in metabolic pathway activity. Cells were treated for 3 and 24 h with each label prior to metabolite extraction. Analysis of RNA, protein, and metabolite abundances was performed similarly by treating the cells for 3 and 24 h with 3FC medium prepared with customized DMEM/F12 without ^{13}C label and conditioned according to the treatment. All cell culture experiments were performed with n = 4 replicates.

2.2. Lipid staining and droplet size determination

Oil Red O staining and DAPI/Nile red staining were used to assess lipid accumulation [42]. Briefly, cells were washed with PBS and fixed with 4 % formaldehyde for 3 h at RT. After removing the formaldehyde solution, cells were again washed with PBS and subsequently stained with 1 µg/mL DAPI, 1 µg/mL Nile red, and 0.2 % (w/v) saponin in PBS for 15 min. After washing with PBS 3x, the fluorescence was recorded at 360/485 nm (E_x/E_m) for DAPI and 485/530 nm (E_x/E_m) for Nile red on a *Synergy*™ HT plate reader (BioTek, Winooski, VT, USA). The non-polar lipid concentration (Nile red fluorescence) is expressed as averaged relative fluorescence units (RFU) in % of the untreated solvent control. For visualization of lipids *via* Oil Red O staining, fixed cells were stained with filtered Oil Red O working solution (0.1 % w/v in 40 % isopropanol) for 30 min at RT, followed by 3x washing with PBS. Images of stained cells in PBS were captured at 10 × magnification using a VisiScope® IT415 PH equipped with a VisiCam® P6 digital camera (VWR, Radnor, PA, USA). The lipid droplet area of the treated mature adipocytes was assessed manually 24 h after incubation with conditioned DMEM/F12 without ^{13}C label in ImageJ (NIH, Bethesda, MD, USA) by analyzing 4 images per treatment.

2.3. Extraction of DINCH, MINCH, intracellular, and extracellular metabolites

Following treatment, 1 mL medium from each condition was collected and centrifuged at 10,000 g and 4 °C for 10 min. After

transferring 300 µL of the supernatant into a new tube, the metabolites were extracted by MeOH/chloroform/water (1/1/1), (v/v/v). MeOH (-20 °C) and ice-cold H_2O were spiked with 100 nM MEHP and 40 µM d6-glutarate, respectively. The extraction mixture was shaken at 1.400 rpm and 4 °C for 20 min and subsequently centrifuged for 10 min at 18,000 g and 4 °C. The polar and non-polar fractions were collected and evaporated to complete dryness (Concentrator plus, Eppendorf, Hamburg, Germany). After removing the supernatant, the SGBS cells were washed twice with 1 mL NaCl. Subsequently, the metabolism was quenched by adding MeOH (-20 °C) with 100 nM MEHP and ice-cold H_2O with 10 µM d6-glutarate to the cells in equal amounts. Cells were scraped and transferred into a new tube with chloroform (-20 °C). Samples were shaken (1400 rpm, 4 °C, 20 min) and subsequently centrifuged at 18,000 g and 4 °C for 5 min. Both the polar and non-polar fractions were collected and evaporated to complete dryness (Concentrator plus, Eppendorf, Hamburg, Germany). All samples were stored at −80 °C until further analysis.

2.4. Targeted LC-MS/MS measurement

Extracted metabolites in the polar fraction from supernatant and cell pellet were analyzed by an adapted LC-MS/MS method described by Buescher et al. [65]. Each sample from the supernatant and cell pellet was resuspended in 112.5 µl and 80 µl H_2O, respectively. Prior to measurement, 10 µl was injected onto an Agilent 1290 II Infinity UPLC system (Agilent Technologies Inc., Santa Clara, CA, USA) coupled on-line with a QTRAP® 6500 + mass spectrometer (Sciex, Framingham, USA). Metabolites were separated on an XSelect HSS T3 XP column (2.1 ×150 mm, 2.5 µm, 100 Å; Waters, Milford, MA, USA) connected to an XP VanGuard® cartridge (HSS T3, 2.1 ×5 mm, 2.5 µM; Waters, Milford, MA, USA). Mobile phase A and mobile phase B were 10 mM tributylamine, 10 mM acetic acid, 5 % methanol, and 2 % 2-propanol (pH 7.1) in water and 100 % 2-propanol, respectively. The chromatographic non-linear gradient is detailed in Table S1. The autosampler was set at 5 °C, and the column oven was kept at 40 °C. Mass spectrometric measurement was performed in negative ionization mode. For identification and quantitation, a scheduled multiple reaction monitoring (MRM) method was used with specific transitions for each metabolite and isotopologue. Data acquisition was performed using the Analyst® software (v. 1.7.0), and peak integration was done in SciexOS® Software (v. 3.0.0, Sciex). All isotopologue measurement values were corrected for 1.1 % of ^{13}C-natural abundance by the R-based IsoCorrectoR tool [66].

2.5. Quantification of DINCH, MINCH, and secondary metabolites

Prior to measurement, non-polar fractions of both the extracted supernatant and cell pellets were re-dissolved in 35 µL MeOH, followed by 35 µL H2O. Each sample (10 µl) was injected into an Agilent 1290 II Infinity UPLC system (Agilent Technologies Inc., Santa Clara, CA, USA) coupled on-line with a QTRAP® 6500 + mass spectrometer (Sciex, Framingham, USA). Chromatographic separation was achieved at 40 °C with an Acquity UPLC BEH Shield RP18 column (2.1 mm×100 mm, 1.7 µm, 130 Å) connected to a VanGuard® precolumn (Acquity UPLC BEH Shield RP18, 2.1 mm×5 mm, 1.7 µm) with A: water + 0.05 % formic acid and B: ACN + 0.05 % formic acid as mobile phases. The chromatographic gradient was as follows: 0–1.0 min at 20 % B with 0.4 mL/min, 1.0–2.5 min 20–50 % B with 0.4 mL/min, 2.5–6.5 min 50–95 % B with 0.4–0.6 mL/min, 6.5–10.0 min at 95 % B with 0.6 mL/min, 10.0–11.0 min 95–20 % B with 0.6–0.4 mL/min, 11.0–13.0 min at 20 % B with 0.4 mL/min. A scheduled MRM method was used with specific precursor/fragment pairs for all compounds. While mass spectrometric measurement for DINCH was performed in positive ionization mode, its metabolites and MEHP were measured in negative ionization mode. Data acquisition was performed using the Analyst® software (v. 1.7.0), and peak integration was done in SciexOS® Software (v. 3.0.0, Sciex). The limit of detection and limit of quantification for DINCH and its metabolites are listed in Table S2. Note that although stringent washing steps of the cell pellets before extraction were applied, it cannot be excluded that extracellularly bound chemicals partly contributed to the measured intracellular concentration of DINCH and its metabolites.

2.6. Quantitative real-time PCR (qPCR)

RNA isolation from treated mature SGBS (24 h after incubation with conditioned DMEM/F12 without ^{13}C label on day 20: control, rosiglitazone, and 10 µM MINCH) was done using RNeasy Lipid Tissue Mini kit (Qiagen, Hilden, Germany) as specified by the manufacturer. qPCR was performed using the LightCycler System LC480 and LightCycler-DNA Master SYBR Green I Kit (Roche, Mannheim, Germany). Adipocyte gene expression was calculated by the ΔΔCT method and normalized to ubiquitin C (*UBC)* levels. Relative gene expression values were depicted as fold changes to the control treatment, respectively. Primer sequences are listed in Table S3.

2.7. SDS-PAGE and western blot

For isolation and quantification of proteins, treated mature SGBS (24 h after incubation with conditioned DMEM/F12 without ^{13}C label on day 20: control, rosiglitazone, and 10 µM MINCH) were collected on ice after adding 60 µL/6-well protein extraction buffer (RIPA, 150 mM NaCl, 10 mM TRIS pH 7.2, 0.1 % SDS, 1 % Triton X-100, 1 % sodium deoxycholate and 5 mM EDTA) completed with protease- and phosphatase inhibitors (Roche), and transferred into 1.5 mL Eppendorf tubes. Samples were homogenized by 3 × 15 s in the ultrasonic bath, followed by incubation at 6 °C for 30 min, and centrifugation (16,000 rpm, 4 °C, 15 min). The total protein concentration of lysate supernatants was determined using a bicinchoninic acid (BCA) assay according to the manufacturer's instructions (Pierce; Thermo Fisher Scientific, Waltham, MA, USA). For immunoblotting, 40 µg of total protein after pooling of the four replicates of each condition (control, rosiglitazone, and 10 µM MINCH) was subjected to SDS polyacrylamide gel electrophoresis (in triplicates for each condition) and subsequently transferred to a nitrocellulose membrane using the tank blot method overnight. Membranes were blocked with 3 % BSA for 1 h at room temperature, followed by primary antibody incubation at 4 °C overnight. Specific HRP-coupled secondary antibodies were used, and chemiluminescence was detected in the G:BOX documentation system (Syngene, Cambridge, UK), followed by densitometric quantification using the GeneTools software (Syngene). Relative protein concentrations were depicted as fold change compared to the control treatment after normalization to β-actin (ACTB). The following primary antibodies were used: from Cell Signaling Technologies (Danvers, MA, USA): pHSL (Ser660) (#45804); HSL (#4107), anti-rabbit-HRP (#7074), anti-mouse-HRP (#7076); from Abcam (Cambridge, UK): UCP1 (ab10983); from Sigma-Aldrich (St. Louis, MO, USA): ACTB (#A1978), from Thermo Fisher Scientific: OXPHOS (#45–8099).

2.8. Measurement of mitochondrial respiration

SGBS preadipocytes (5000 per well) were seeded into XF96 plates, and adipogenesis was then induced in confluent preadipocytes as described in 2.1. Starting from day 12 of differentiation SGBS-adipocytes were treated with 2 µM Rosi, 10 µM MINCH or solvent control as described in 2.1.

Mitochondrial stress test (MST) was performed according to the manufacturer's protocol on day 20 in differentiated adipocytes. Cells were washed two times with Seahorse XF DMEM medium, pH 7.4 supplemented with 2 mM glutamine, 1 mM pyruvate and 10 mM glucose and then incubated for 1 h at 37 °C in an incubator without CO_2. Concentration of the injections and loading of port were as followed: (A) 2 µM oligomycin; (B) 2 µM carbonylcyanide-p-trifluoromethoxyphenylhydrazone and (C) 0.5 µM rotenone/antimycin

A. The oxygen consumption rate (OCR) was measured by 3 min mix and 2 min measure (XF96, Seahorse XF Pro Analyzer, Agilent Technologies Inc., Santa Clara, CA, USA). Analysis was performed with Wave Pro (v10.1.0.). To minimize the variability of the OCR, we optimized the seeding to the same cell number and adipogenesis was induced in fully confluent preadipocytes. Therefore, no normalization was performed [67]. Key parameters of mitochondrial respiration were calculated and analyzed according to manufacturer's instructions.

2.9. Metabolite normalization and statistical analysis

Data was analyzed and visualized with the use of GraphPad Prism (v 10.4.1, La Jolla, CA, USA) and R software (v 4.0.5). Intracellular and extracellular metabolite abundances were normalized to the DAPI-stained DNA content (DAPI fluorescence) as described in Goerdeler et al. [57]. For the one-way ANOVA analysis (lipid accumulation, lipid droplet area, mRNA expression, and protein levels) GraphPad Prism automatically performed a Brown-Forsythe test to verify equality of variances. As the samples met the assumption, a one-way ANOVA test followed by Dunnett's post-hoc test was applied to compare each treatment group against the untreated control. For metabolite abundances, ^{13}C isotopologue abundances, and ^{13}C fractional contributions variance homogeneity was not assumed. Therefore, a Welch ANOVA test was selected, followed by a Games-Howell post-hoc test which is robust to unequal variances and sample sizes and offers greater power for large-scale comparisons. For isotopologue ratios used in metabolic flux assessments and for all parameters analyzed within the Seahorse XF assay a Welch ANOVA test followed by a Dunnett's T3 post-hoc test was applied, as only comparisons against the untreated control of the respective time point were of interest. Dunnett's T3 was chosen as a more conservative test to minimize the risk of overestimating significance for these targeted comparisons. The PPP to glucose metabolism ratio was calculated based on the labeling pattern of extracellular lactate after [1,2-^{13}C]glucose incubation according to equation 3 described in Morken et al. [60]. Obtaining positional information on the ^{13}C label of lactate was possible due to the loss of the CO_2 group of the analyzed fragment ion. Grubb's outlier test with $\alpha = 0.05$ was performed to identify potential outliers. All values are expressed as mean ± standard deviation (SD), if not otherwise mentioned. Values for the concentrations of DINCH, MINCH, and the secondary metabolites, the metabolite abundances, the ^{13}C isotopologue abundances, and the ^{13}C fractional contributions can be found in the Supplementary Data.

3. Results

3.1. Mature adipocytes show higher intracellular concentrations and biotransformation capacity

To investigate cellular uptake and biotransformation of DINCH/MINCH prior to the assessment of the effects on the metabolism, the concentrations of DINCH, MINCH, and the secondary metabolites in the cell culture medium and exposed preadipocytes and mature adipocytes were measured. As observed previously, the 10 μM nominal concentration of DINCH resulted in approximately 500 nM measured actual concentration in the conditioned cell culture medium (Fig. 1A), whereas the 10 nM and 10 μM nominal concentrations of MINCH corresponded well with the measured concentration (11.7 nM and 9.6 μM, respectively; Fig. 1B and C). Concentrations of DINCH and MINCH in the cell medium decreased after incubation with SGBS cells for 3 h and 24 h (Fig. 1A, B, and C). Analysis of the concentrations in the cell pellets confirmed that this decrease is at least partly attributed to cellular uptake of DINCH and MINCH (Fig. 1D, E, and F). Interestingly, intracellular concentrations for both doses of MINCH were higher in the treated mature adipocytes compared to the treated preadipocytes (Fig. 1E and F). Assessment of biotransformation of DINCH by mature adipocytes showed an increase of extra- and intracellular levels of MINCH to 1.6 nM and 4.0 pmol/10^6 cells after 24 h, respectively (Fig. 1G and H). Further biotransformation of MINCH to OH-MINCH was observed in 10 μM MINCH-treated cells. The OH-MINCH levels in mature adipocytes were 2- to 10-fold higher extracellularly and 3-fold higher intracellularly compared to preadipocytes (Fig. 1I and J). Additionally, low levels of oxo-MINCH were detected after 24 h extracellularly in 10 μM MINCH-treated mature adipocytes, but not intracellularly, and not in treated preadipocytes (Fig. 1K).

3.2. Induction of lipid accumulation is accompanied by elevated glycolysis and PPP in MINCH-treated preadipocytes

To assess the effects of MINCH on adipogenesis, preadipocytes were treated with two different doses of MINCH (10 nM and 10 μM) for 12 days (Figure S1A). Analysis of the lipid accumulation of treated preadipocytes incubated on day 12 for 3 h and 24 h in conditioned medium without isotopic tracer confirmed the previously observed adipogenic potential of MINCH in the μM concentration range (Figure S2A and B) [42,57]. While no effect was observed by the 10 nM MINCH treatment, the lipid content was elevated by 157 % at both time points compared to the untreated control by 10 μM dose of MINCH, but to a lesser extent compared to the rosiglitazone-differentiated positive control (Rosi 254 % of solvent ctrl; Figure S2B). DNA content by DAPI staining showed a slight increase by the 10 μM MINCH (115 % of solvent ctrl) and rosiglitazone (145 % of solvent ctrl) treatment and confirmed the absence of effects on cell viability by the tracer medium (Figure S2C).

After analyzing the changes in lipid and DNA content, the effects on glycolysis and pentose phosphate pathway (PPP) activity were investigated 3 and 24 h after incubation with medium without isotopic tracer on day 12. Rosiglitazone-differentiated preadipocytes showed strongly elevated metabolite levels of upper glycolysis to glyceraldehyde 3-phosphate (G3P), lower glycolysis, and the pentose phosphate pathway (PPP), as well as increased lactate secretion at 3 and 24 h (Fig. 2A and S3). Similarly, in 10 μM MINCH-treated cells, increased levels of lower glycolysis metabolites and elevated lactate secretion were observed, but almost no differences in metabolite levels of upper glycolysis and the PPP (Fig. 2A and Figure S3). In contrast, no changes in metabolite levels were observed after 10 nM MINCH treatment (Fig. 2A and Figure S3). Analysis of the labeling pattern after [U-^{13}C]glucose incubation revealed an increased ^{13}C labeling of measured metabolites of upper and lower glycolysis and extracellular lactate after 3 and 24 h in rosiglitazone-differentiated cells, evident by the elevated M+ 6 or M+ 3 isotopologues and fractional contributions (Fig. 2A and Figure S4 and S5). Together, the data suggest an elevated glycolytic flux in rosiglitazone-differentiated cells, as already indicated by the strong increase in metabolite levels in comparison to untreated control cells. Similar to rosiglitazone-differentiated cells, 10 μM MINCH increased [U-^{13}C]glucose labeling to metabolites of lower glycolysis and extracellular lactate at 3 and 24 h, indicating an elevated glycolytic flux (Fig. 2B and Figure S5). In contrast, 10 nM MINCH did not induce alterations in metabolites of lower glycolysis. However, the small increase in extracellular lactate labeling might suggest a minor upregulation of glycolytic activity for lactate production (Fig. 2B and Figure S5).

Labeling data from the PPP showed an increased labeling contribution from [U-^{13}C]glucose to ribulose 5-phosphate (Ru5P) due to the elevated M+ 5 Ru5P at 3 and 24 h in rosiglitazone-differentiated cells (Fig. 2A and B and Figure S4 and S5). Again, similar to the elevated metabolite levels, this suggests an increased flux through the PPP. As for rosiglitazone treatment, increased labeling of Ru5P at 24 h indicated increased PPP flux in the 10 μM MINCH treatment, although to a lesser extent (Fig. 2B). No changes in PPP activity were observed in the 10 nM MINCH treatment (Fig. 2B). Analysis after [1,2-^{13}C]glucose incubation supports the higher glycolytic activity for rosiglitazone- and 10 μM MINCH treatment as evidenced by the reduced M+ 0 and significantly increased M+ 2 in pyruvate and extracellular lactate (Figure S6). Similarly, the higher PPP activity of rosiglitazone and 10 μM MINCH

treatment is supported by the decreased M+ 0 and increased M+ 1 (rosiglitazone) or M+ 3 (10 μM MINCH) of Ru5P at 24 h (Figure S6). [1,2-^{1} ^{3}C]glucose labeling was used to assess the contribution of the pentose phosphate pathway (PPP) to total glucose metabolism (glycolysis + PPP), based on the calculated PPP/glucose metabolism ratio. This analysis revealed an increased PPP contribution in rosiglitazone treatment at 3 and 24 h (Fig. 2C). In contrast, after 10 μM MINCH treatment, no changes or even a minor decrease in the PPP/glucose metabolism ratio were observed at 3 and 24 h, respectively (Fig. 2C).

To complement the analysis of glycolysis and PPP, we next assessed the effects on glyceroneogenesis, i.e., the synthesis of glycerol 3-phosphate (Gro3P) from pyruvate *via* an abbreviated form of

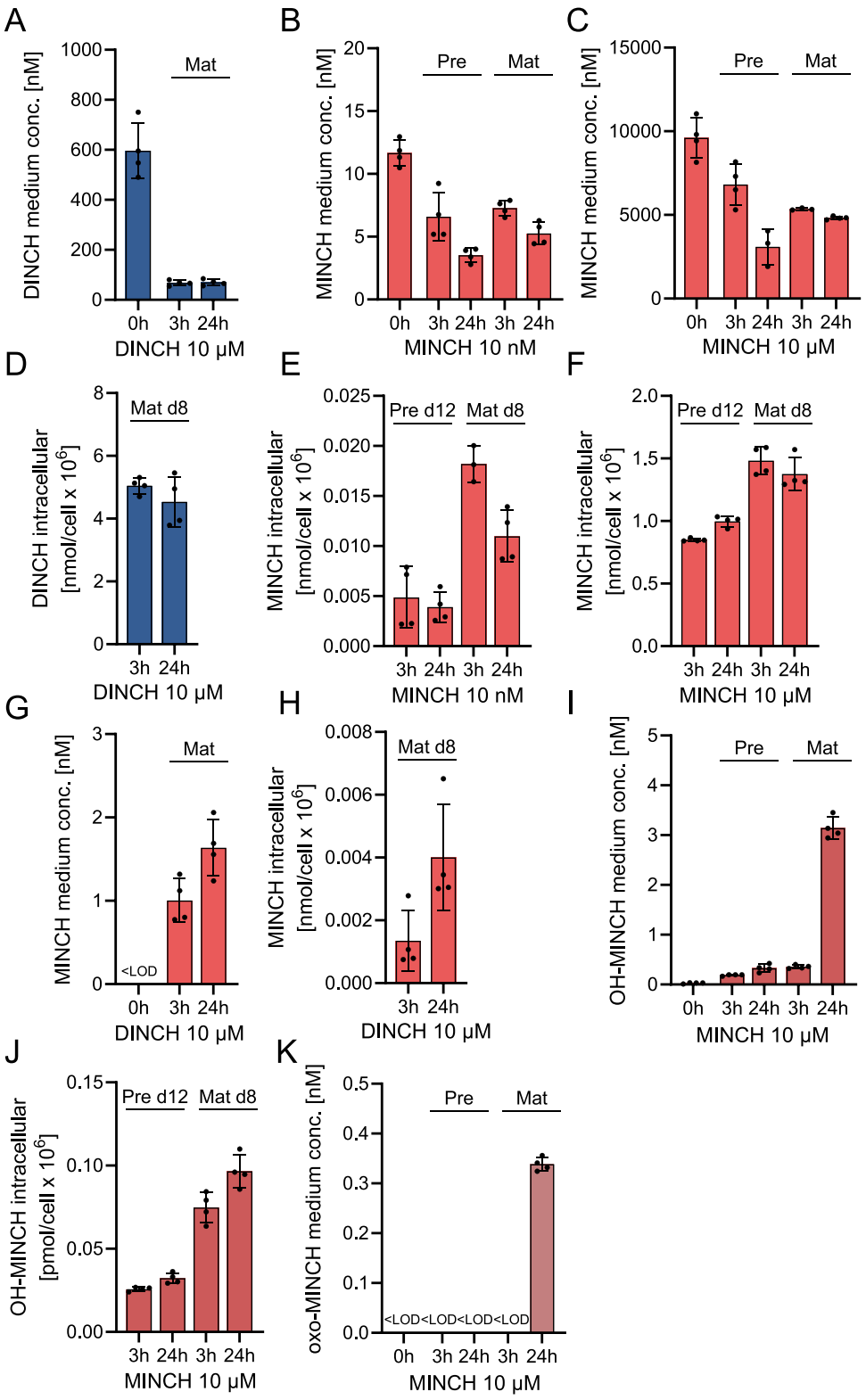

(caption on next page)

Fig. 1. Concentration analysis of DINCH- and MINCH-treated preadipocytes and mature adipocytes. (A) DINCH concentration in the medium supernatant (10 μM applied nominal concentration) before and 3 and 24 h after mature SGBS treatment on day 20. (B) MINCH concentration (10 μM applied nominal concentration) in the medium supernatant before and 3 and 24 h after preadipocyte (Pre) and mature (Mat) SGBS treatment on day 12 and day 20, respectively. (C) MINCH concentration (10 nM applied nominal concentration) in the medium supernatant before and 3 or 24 h after preadipocyte and mature SGBS treatment on day 12 and day 20, respectively. (D) Intracellular concentration of DINCH after 8 days of treatment of mature SGBS cells with 10 μM DINCH and additional incubation with conditioned DMEM/F12 without ^{13}C label for 3 and 24 h on day 20. (E) Intracellular concentration of MINCH after 12 days of preadipocyte treatment and 8 days of mature adipocyte treatment with 10 μM MINCH and additional incubation with conditioned DMEM/F12 without ^{13}C label for 3 and 24 h on day 12 and day 20, respectively. (F) Intracellular concentration of MINCH after 12 days of preadipocyte treatment and 8 days of mature adipocyte treatment with 10 nM MINCH and additional incubation with conditioned DMEM/F12 without ^{13}C label for 3 and 24 h on day 12 and day 20, respectively. (G) MINCH concentration in the 10 μM DINCH medium supernatant before and 3 and 24 h after mature SGBS treatment on day 20. (H) Intracellular concentration of MINCH after 8 days of treatment of mature SGBS cells with 10 μM DINCH and additional 3 and 24 h incubation with conditioned DMEM/F12 without ^{13}C label on day 20. (I) OH-MINCH concentration in the 10 μM MINCH medium supernatant before and 3 and 24 h after preadipocyte treatment on day 12 and mature SGBS treatment on day 20, respectively. (J) Intracellular concentration of OH-MINCH after 12 days of preadipocyte treatment and 8 days of mature adipocyte treatment with 10 μM MINCH and additional incubation with conditioned DMEM/F12 without ^{13}C label for 3 and 24 h on day 12 and day 20, respectively. (K) oxo-MINCH concentration in the 10 μM MINCH medium supernatant before and 3 and 24 h after preadipocyte treatment on day 12 and mature SGBS treatment on day 20, respectively. All values are expressed as mean ± SD (n = 4). Intracellular values were normalized to the DAPI-measured DNA content.

gluconeogenesis, using [U-$^{1\ 3}$C]glutamine labeling. Since glutamine-derived carbon enters this pathway through the TCA cycle and subsequent conversion to pyruvate, we compared the $^{1\ 3}$C labeling of Gro3P to that of pyruvate as a measure of glyceroneogenesis activity. Notably, metabolites of the lower glycolysis pathway showed only minimal labeling from glutamine across all treatments, indicating limited glutamine contribution to this part of metabolism under the tested conditions (Fig. 2B and Figure S5). Rosiglitazone-differentiated cells showed a decreased glyceroneogenesis activity at 24 h (Fig. 2C), in line with the decreased labeling contribution to Gro3P from glutamine and increased contribution from glucose (Figure S5). In contrast, in 10 μM MINCH-treated cells, a trend towards transiently elevated glyceroneogenesis activity was observed at 3 h ($p = 0.059$; Fig. 1D), supported by the increased labeling of Gro3P from Gln at 3 h (Figure S5).

3.3. MINCH treatment of preadipocytes switches TCA cycle activity toward lipid synthesis

Downstream of glycolysis, acetyl-CoA serves as a link to the TCA cycle and plays an important role in adipocytes as a critical substrate for fatty acid synthesis [68]. Strongly increased acetyl-CoA levels were observed at both time points in rosiglitazone and 10 μM MINCH-treated cells, together with an elevated extent of labeling from [U-^{13}C]glucose (Fig. 3A and B), suggesting increased flux from glycolysis for acetyl-CoA production. Although no increase in acetyl-CoA levels was observed in 10 nM MINCH-treated cells (Fig. 3A and Figure S3), labeling from [U-^{13}C]glucose was slightly elevated at 3 h (Figure S5), but not at 24 h (Fig. 3B). [U-^{13}C]glutamine labeling data revealed elevated contribution in rosiglitazone-differentiated and 10 μM MINCH at 3 and 24 h (Fig. 3B). Interestingly, analysis of the reductive isocitrate dehydrogenase (IDH) flux by the ratio of M+ 5 citrate to M+ 5 glutamate as an indicator for reductive glutaminolysis showed a transient upregulation of reductive IDH flux at 3 h in rosiglitazone and 10 μM MINCH treatment (Fig. 3C).

Similar to acetyl-CoA levels, metabolite abundances of mainly all TCA-cycle metabolites were increased at 3 and 24 h in rosiglitazone and partly in 10 μM MINCH treatment, whereas no changes were observed in 10 nM MINCH treatment (Figure S3). Comparison of the [U-^{13}C]glucose and [U-^{13}C]glutamine labeling contribution to the TCA cycle metabolites showed that for 10 nM MINCH-treated cells, similar to the untreated control, glutamine was the main labeling source (Fig. 3B and Figure S5). In contrast, rosiglitazone-treated cells showed a reduced labeling from glutamine and an increased labeling from glucose, with an even higher contribution of glucose labeling in citrate, *cis*-aconitate, malate, and aspartate, which serves as a surrogate for oxaloacetate, at 24 h (Fig. 3B and Figure S5). Similarly, although in 10 μM MINCH-treated cells glutamine was the main labeling source, the extent of labeling from glucose was increased for all metabolites of the TCA cycle and nearly similar to glutamine labeling for malate and aspartate after 24 h (Fig. 3B and Figure S5). The observed pronounced increase in the [U-^{13}C]glucose labeling of malate and aspartate in rosiglitazone and MINCH treatment was mainly driven by an increase in the M+ 3 isotopologue (Fig. 3A and B), which can be either formed by anaplerotic contribution of M+ 3 pyruvate to oxaloacetate *via* pyruvate carboxylase or from M+ 2 acetyl-CoA by multiple rounds of oxidation in the TCA cycle [69]. Since the comparable low levels of M+ 3 succinate in 10 μM MINCH treatment (0.7 % at 24 h) and rosiglitazone-treatment (4.6 % at 24 h) indicate minimal contribution to M+ 3 malate from multiple TCA cycle oxidation rounds, this suggests an increase of pyruvate carboxylase flux in both treatments (Fig. 3A and Figure S4). This is supported by the increase in M+ 5 citrate in rosiglitazone and 10 μM MINCH-treated cells at 3 and 24 h (Fig. 3A and Figure S4), which is formed when M+ 3 oxaloacetate from pyruvate anaplerosis is subsequently combined with M+ 2 acetyl-CoA in the TCA cycle. Although no overall increase in [U-^{13}C]glucose labeling contribution to TCA cycle metabolites was observed as with rosiglitazone treatment and 10 μM MINCH treatment, increased glucose labeling of malate, caused by an increased M+ 3 isotopologue at 3 and 24 h, and increased M+ 3 aspartate at 3 h already indicates a slight upregulation of pyruvate carboxylase flux in 10 nM MINCH treated cells (Fig. 3A and B and Figure S4).

Contrary to the transiently increased reductive IDH flux, there is a decreased oxidative TCA cycle flux as the ratio of the M+ 4 citrate to M+ 5 glutamate was decreased in rosiglitazone and 10 μM MINCH treatment 3 h, but not 24 h, after [U-^{13}C]glutamine labeling (Fig. 3D). In addition to the transiently decreased oxidative TCA cycle flux, the reduced M+ 3 glutamate to M+ 5 glutamate ratio 3 h and 24 h after [U-^{13}C]glutamine labeling in rosiglitazone and 10 μM treatment indicates decreased cycling of glutamate through the oxidative TCA cycle (Fig. 3E). No changes in the oxidative TCA flux and cycling activity were observed in 10 nM MINCH-treated cells.

3.4. MINCH treatment of mature adipocytes promoted a metabolic shift towards increased glycolysis and glyceroneogenesis

In addition to assessing the effects of MINCH on adipogenesis, we analyzed its effects on mature adipocytes, as these are crucial for evaluating long-term effects of metabolism-disrupting chemicals due to the relatively low turnover rate of adipocytes in adults (~8 % per year) [70]. Fully differentiated SGBS cells were treated from day 12 to day 20 with either DINCH (10 μM), MINCH (10 nM and 10 μM), or rosiglitazone (2 μM) (Figure S1B). On day 20, cells were incubated for 3 h and 24 h in medium without (phenotypic analysis, metabolite abundances) or with isotopic tracer for 3 or 24 h, similar to exposed preadipocytes. Phenotypic analysis of mature adipocytes showed decreased lipid content in 10 μM MINCH-treated cells (Figure S7A and B) and increased DNA content in rosiglitazone-treated cells (Figure S7C), resulting in decreased lipid content normalized to the DNA content in both treatments (Figure S7D). No phenotypic alterations for DINCH and 10 nM MINCH treatment were observed (Figure S7). The analysis of changes in

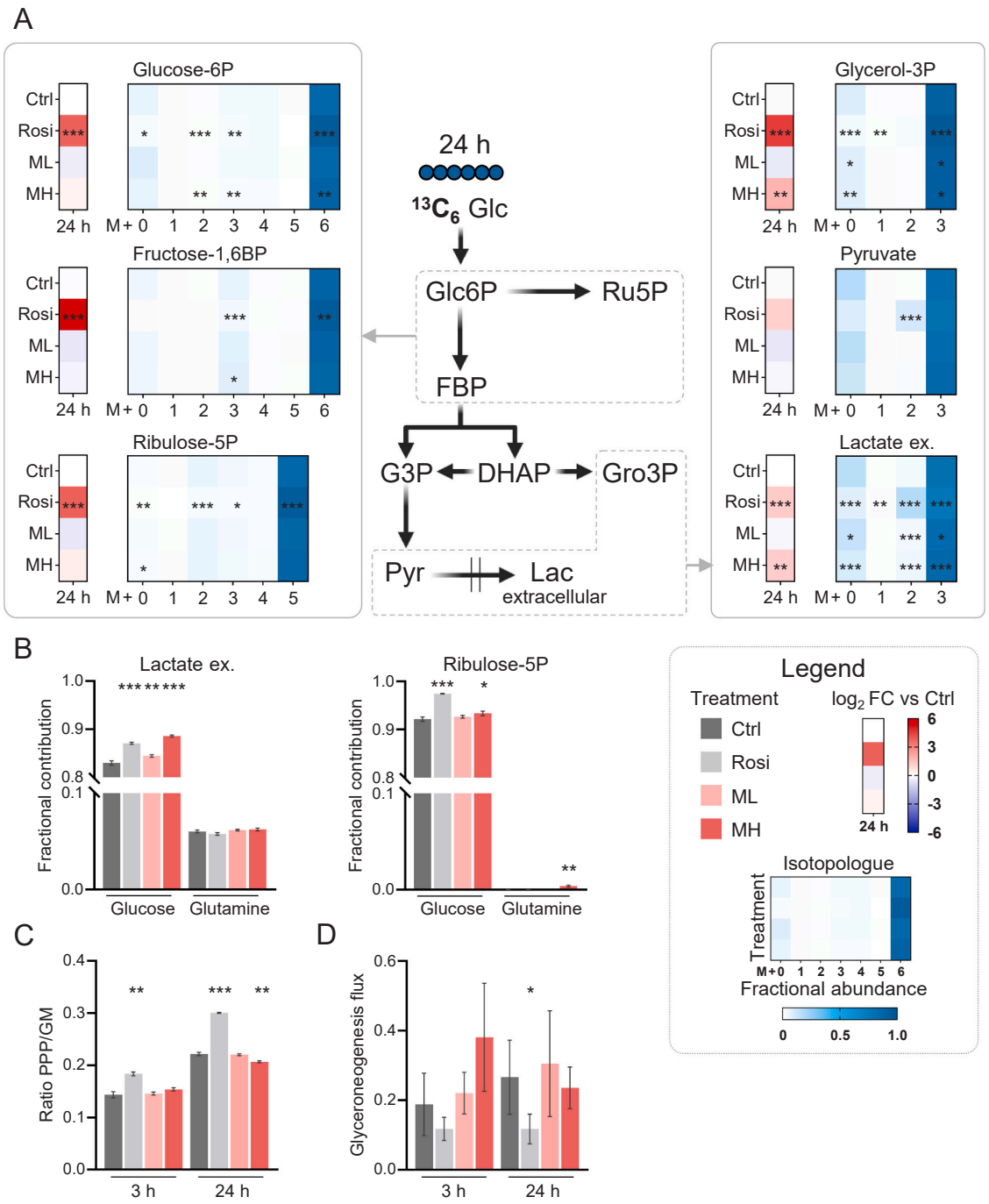

Fig. 2. Effects of MINCH on glycolysis, PPP, and glyceroneogenesis activity of treated SGBS preadipocytes. (A) Metabolite abundances and isotopologue enrichment from [U-^{13}C]glucose labeling of selected metabolites of the glycolysis and PPP of MINCH-treated SGBS preadipocytes (ML – MINCH Low (10 nM) and MH – MINCH High (10 μM)) and SGBS cells treated with rosiglitazone (Rosi) 24 h after incubation with conditioned DMEM/F12 with (isotopologue enrichment) or without (abundances) ^{13}C label on day 12. Metabolite abundances are presented as $\log_2$ fold changes (FC) compared to the untreated control and isotopologue enrichments are represented as relative fractional abundances after correction of natural isotope abundance. Metabolite levels were normalized to the DNA content determined by DAPI fluorescence. (B) ^{13}C fractional contribution from glucose and glutamine to extracellular lactate and ribulose 5-phosphate of MINCH-treated, rosiglitazone-differentiated, and untreated control cells 24 h after labeling with [U-^{13}C]glucose and [U-^{13}C]glutamine, respectively. (C) PPP contribution to the total glucose metabolism (i.e., glycolysis and PPP together) of MINCH-treated, rosiglitazone-differentiated, and untreated control cells determined by labeling with [1,2-^{13}C] glucose. (D) Glyceroneogenesis activity of MINCH-treated, rosiglitazone-differentiated, and untreated control cells assessed after [U-^{13}C]glutamine labeling by the ratio of the M+ 2 isotopologue of glycerol 3-phosphate to the M+ 2 isotopologue of pyruvate and the ratio of the M+ 3 isotopologue of glycerol 3-phosphate to the M+ 3 isotopologue of pyruvate. Values are expressed as mean ± SD (n = 4). Welch ANOVA followed by Games-Howell (A, B) and Dunnett's T3 (C, D) post-hoc test was performed to calculate statistical significance, and significant changes are displayed compared to the untreated control of the respective time point; *$p < 0.05$, **$p < 0.01$, ***$p < 0.001$. DHAP – dihydroxyacetone phosphate, FBP – fructose 1,6-bisphosphate, GM – glucose metabolism, G6P – glucose 6-phosphate, G3P – glyceraldehyde 3-phosphate, Gro3P – glycerol 3-phosphate, Lac – lactate, Pyr – pyruvate, and Ru5P – ribulose 5-phosphate.

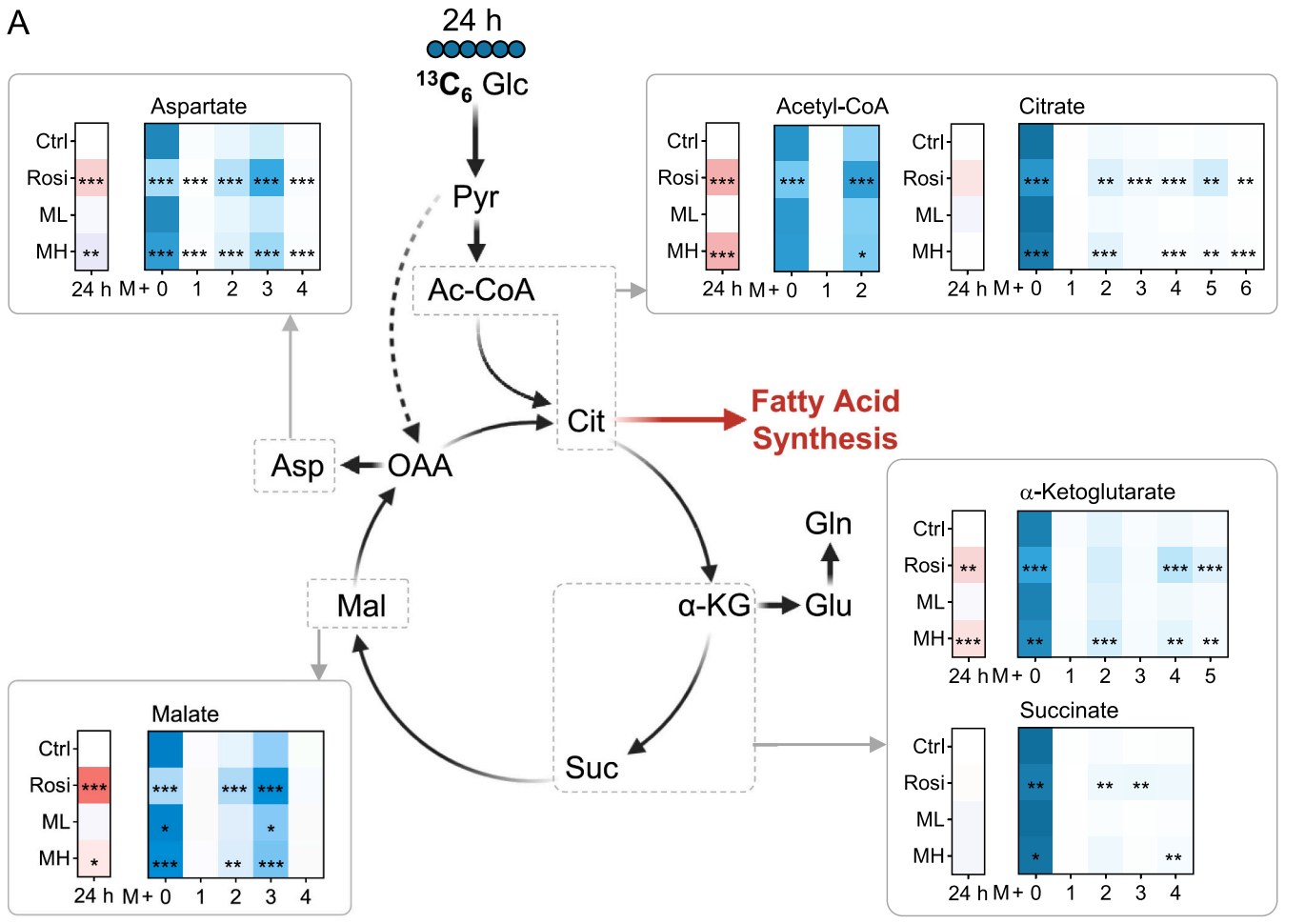

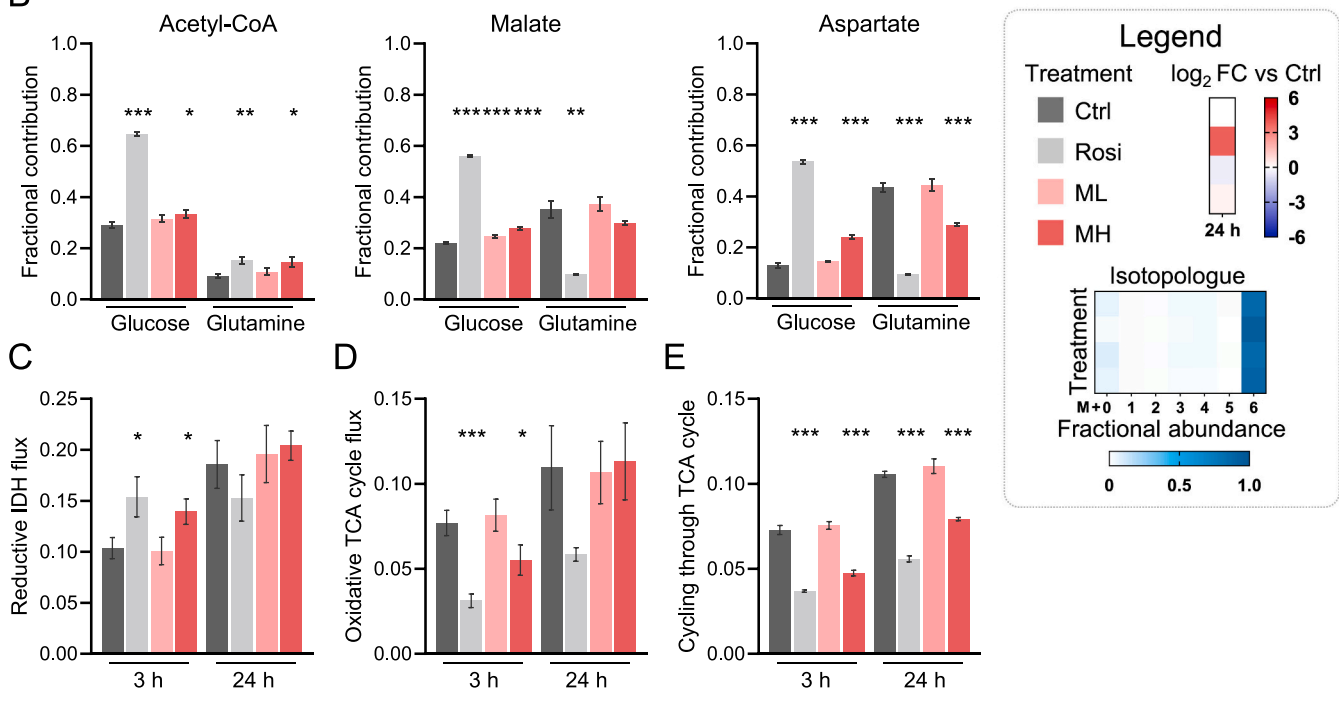

(caption on next page)

Fig. 3. Effects of MINCH on the TCA cycle activity of treated SGBS preadipocytes. (A) Metabolite abundances and isotopologue enrichment from [U-^{13}C]glucose labeling of selected metabolites of the TCA cycle and acetyl-CoA of MINCH-treated SGBS preadipocytes (ML – MINCH Low (10 nM) and MH – MINCH High (10 μM)) and SGBS cells treated with rosiglitazone (Rosi) 24 h after incubation with conditioned DMEM/F12 with (isotopologue enrichment) or without (abundances) ^{13}C label on day 12. Metabolite abundances are presented as $\log_2$ fold changes (FC) compared to the untreated control and isotopologue enrichments are represented as relative fractional abundances after correction of natural isotope abundance. Metabolite levels were normalized to the DNA content determined by DAPI fluorescence. (B) ^{13}C fractional contribution from glucose and glutamine to acetyl-CoA, malate, and aspartate of MINCH-treated, rosiglitazone-differentiated, and untreated control cells 24 h after labeling with [U-^{13}C]glucose and [U-^{13}C]glutamine, respectively. (C) Reductive isocitrate dehydrogenase (IDH) flux of MINCH-treated, rosiglitazone-differentiated, and untreated control cells assessed after labeling with [U-^{13}C]glutamine by the ratio of the M+ 3 isotopologue of citrate to the M+ 5 isotopologue of glutamate. (D) Oxidative TCA cycle flux of MINCH-treated, rosiglitazone-differentiated, and untreated control cells after labeling with [U-^{13}C]glutamine determined by the ratio of the M+ 4 isotopologue of citrate to the M+ 5 isotopologue of glutamate. (E) Cycling of glutamate through the TCA cycle of MINCH-treated, rosiglitazone-differentiated, and untreated control cells, assessed after labeling with [U-^{13}C]glutamine by the ratio of the M+ 3 isotopologue of glutamate to the M+ 5 isotopologue of glutamate. Values are expressed as mean ± SD (n = 4). Welch ANOVA followed by Games-Howell (A, B) and Dunnett's T3 (C, D, E) post-hoc test was performed to calculate statistical significance, and significant changes are displayed compared to the untreated control of the respective time point; *$p < 0.05$, **$p < 0.01$, ***$p < 0.001$. Ac-CoA – acetyl coenzyme A, Asp – aspartate, Cit – citrate, Gln – glutamine, Glu – glutamate, α-KG – α-ketoglutarate, Mal – malate, OAA – oxaloacetate, Pyr – pyruvate, and Suc – succinate.

metabolite abundances of glycolysis and PPP showed mainly increased metabolite levels of lower glycolysis and elevated secretion of pyruvate at 3 h and decreased metabolite levels of upper glycolysis and PPP at 24 h in rosiglitazone and 10 μM MINCH-treated cells (Fig. 4A and Figure S8). Almost no effects of the 10 nM MINCH and the DINCH treatment were observed (Fig. 4A and Figure S8).

[U-^{13}C]glucose labeling showed slightly decreased labeling from glucose in metabolites of upper and lower glycolysis, evident by the increased M+ 0 and decreased M+ 6 or M+ 3 isotopologues at 3 and 24 h in rosiglitazone and 10 μM MINCH-treated cells (Fig. 4A and B and Figure S9 and S10). In the PPP, labeling contribution from glucose in Ru5P was not increased, but increased M+ 2 and M+ 4 isotopologues were observed in rosiglitazone and 10 μM MINCH treatment at 3 and 24 h (Fig. 4A and B and Figure S9 and S10). In contrast to glucose, labeling contribution from glutamine was elevated in metabolites of glycolysis, PPP, and also Gro3P, suggesting a higher glyceroneogenesis activity in rosiglitazone and 10 μM MINCH treatment (Fig. 4B and Figure S9). Indeed, comparison of the glutamine labeling from Gro3P and pyruvate indicated increased glyceroneogenesis activity at 3 h in 10 μM MINCH treatment and at both time points in rosiglitazone treatment, but not in the other treatments (Fig. 4C).

Extracellular lactate as the endpoint of glycolysis showed a slight increase in the extent of labeling from glucose in rosiglitazone and a more pronounced increase in 10 μM MINCH treatment at 24 h (Fig. 4B). At the same time, while the labeling of lactate from glutamine was elevated in rosiglitazone-treated cells, indicating a higher utilization of glutaminolysis for lactate production, a decreased labeling was observed in 10 μM MINCH-treated cells (Fig. 4B). The increased glycolytic activity in the 10 μM MINCH treatment was supported by the [1,2-^{13}C]glucose labeling data showing elevated M+ 2 labeling in lactate at 24 h (Figure S11). Opposite to 10 μM MINCH, a decrease in M+ 2 lactate, but an increase in M+ 0 and M+ 1 was observed in rosiglitazone-treated cells (Figure S11). This indicates a shift towards higher PPP contribution in rosiglitazone treatment. In line with this, an increased PPP contribution to total glucose metabolism was observed in rosiglitazone-treated cells at 3 and 24 h (Fig. 4D). In contrast, the PPP contribution to the glucose metabolism was not altered in the 10 μM MINCH treatment. However, as the labeling and abundance data indicate a higher glycolytic activity, this suggests a concomitant increase in PPP activity to maintain a stable PPP/glucose metabolism ratio (Fig. 4D). No effects on glycolytic and PPP activity were observed in 10 nM MINCH and DINCH-treated cells (Fig. 4).

3.5. *MINCH-treated mature adipocytes show a source switch for acetyl-CoA synthesis and increased oxidative TCA cycle activity*

Downstream of glycolysis, the analysis of acetyl-CoA abundances in mature adipocytes showed no significant changes in rosiglitazone and 10 μM MINCH treatment (Figure S8), but a strong decrease in the extent of labeling from glucose in rosiglitazone treatment and to a lesser extent in 10 μM MINCH treatment at both time points (Fig. 5A and Figure S9). Since there was no concomitant increase in the labeling from glutamine, but even decreased labeling at 24 h in rosiglitazone and 10 μM MINCH-treated cells (Fig. 5A), this indicates an increased contribution to acetyl-CoA generation from other sources, such as the degradation of branched-chain amino acids or fatty acid β-oxidation. In contrast to rosiglitazone and 10 μM MINCH treatment, no changes in acetyl-CoA contribution were observed in 10 nM MINCH and DINCH treatment (Fig. 5A).

An analysis of the TCA cycle showed bifurcated changes in metabolite abundances by the 10 μM MINCH treatment. The citrate to succinate levels, together with glutamate, were increased at 24 h and partly at 3 h, whereas there was mainly a strong decrease in the fumarate to oxaloacetate levels, together with aspartate at both time points (Figure S8). While similar changes in metabolite abundances were observed in rosiglitazone treatment, almost no changes were observed by 10 nM MINCH and DINCH treatment. Consistent with the metabolite levels, labeling of the TCA cycle metabolites from [U-^{13}C]glucose and [U-^{13}C]glutamine remained nearly unaltered in 10 nM MINCH and DINCH treatment. Similarly, rosiglitazone-treated cells showed almost no changes in labeling of citrate or downstream metabolites up to α-ketoglutarate at either time point, but increased labeling of succinate from glucose at 3 h, together with a more than 2-fold increase in the labeling from glutamine (Fig. 5A and Figure S9). In contrast, 10 μM MINCH-treated cells showed increased labeling contribution from glucose to citrate towards succinate, accompanied by decreased labeling contribution from glutamine at 24 h in α-ketoglutarate and succinate (Fig. 5A and Figure S9). Since less labeling of acetyl-CoA from glucose was observed in rosiglitazone and 10 μM MINCH treatment, the stable to increased glucose labeling from citrate towards succinate suggests an increased flux from acetyl-CoA into the TCA cycle in both treatments.

In line with the bifurcation in metabolite abundances, the [U-^{13}C]glucose and [U-^{13}C]glutamine labeling data revealed that in contrast to labeling from citrate to succinate, there was a significant decrease in the glucose labeling and a concomitant increase in glutamine labeling in malate and aspartate of 10 μM MINCH-treated cells at 3 h (Figure S9). This change in labeling was partly reversed at 24 h with increased glucose labeling in malate, but not in aspartate (Fig. 5A). Similarly, in rosiglitazone treatment, a decreased labeling contribution from glucose and an elevated contribution from glutamine were observed in malate and aspartate at both time points (Fig. 5A and Figure S9). This suggests a higher glutaminolysis flux from glutamine to malate and oxaloacetate in rosiglitazone and 10 μM MINCH treatment. Concomitant with this increase in anaplerotic glutamine contribution, analysis of the M+ 4 citrate to M+ 5 glutamate ratio after incubation with [U-^{13}C]glutamine indicates a transient increase in oxidative TCA cycle flux in rosiglitazone-treated cells at 3 h, but not in 10 μM MINCH-treated cells (Fig. 5B). However, analysis of the M+ 3 glutamate to M+ 5 glutamate after [U-^{13}C]glutamine incubation indicated a transient increase in oxidative cycling of glutamate through the TCA cycle in 10 μM MINCH treatment at 3 h instead (Fig. 5C). Together with the increased flux from

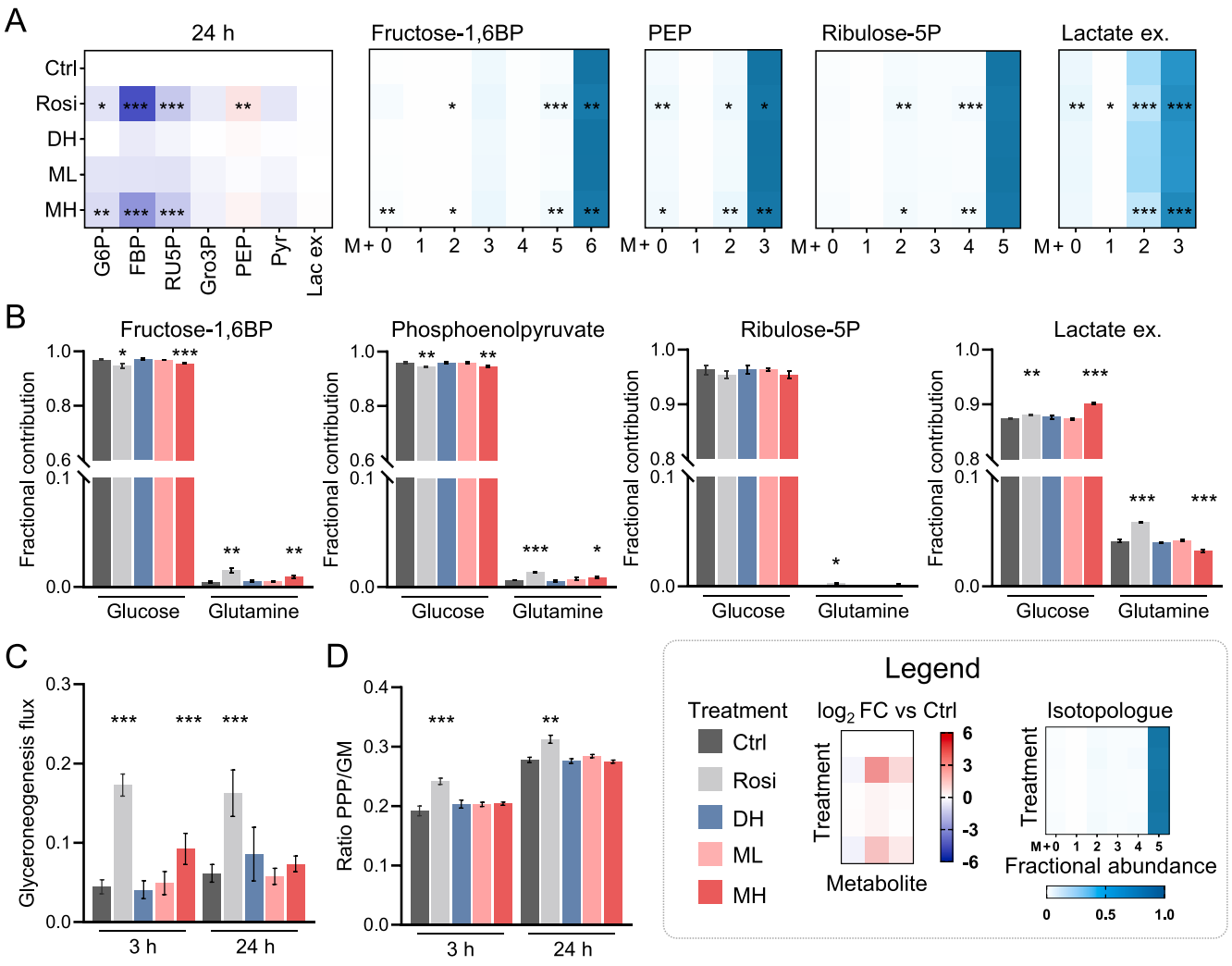

Fig. 4. Effects of DINCH and MINCH on glycolysis, PPP, and glyceroneogenesis activity of treated mature adipocytes. (A) Metabolite abundances of selected metabolites of the glycolysis and PPP and isotopologue enrichment from [U-^{13}C]glucose labeling in ribulose 5-phosphate, glycerol 3-phosphate, and extracellular lactate of DINCH- and MINCH-treated mature SGBS adipocytes (DH – DINCH High (10 μM), ML – MINCH Low (10 nM), and MH – MINCH High (10 μM)) and SGBS cells treated with rosiglitazone (Rosi) 24 h after incubation with conditioned DMEM/F12 with (isotopologue enrichment) or without (abundances) ^{13}C label on day 20. Metabolite abundances are presented as $\log_2$ fold changes (FC) compared to the control and isotopologue enrichments are represented as relative fractional abundances after correction of natural isotope abundance. Metabolite levels were normalized to the DNA content determined by DAPI fluorescence. (B) ^{13}C fractional contribution from glucose and glutamine to fructose 1,6-bisphosphate, ribulose 5-phosphate, phosphoenolpyruvate, and extracellular lactate of DINCH- and MINCH-treated, rosiglitazone-treated, and untreated control cells 24 h after labeling with [U-^{13}C]glucose and [U-^{13}C]glutamine, respectively. (C) Glyceroneogenesis activity of DINCH-, MINCH-, and rosiglitazone-treated cells compared to untreated control cells assessed after [U-^{13}C]glutamine labeling by the ratio of the M+ 2 isotopologue of glycerol 3-phosphate to the M+ 2 isotopologue of pyruvate and the ratio of the M+ 3 isotopologue of glycerol 3-phosphate to the M+ 3 isotopologue of pyruvate. (D) PPP contribution to the total glucose metabolism (i.e., glycolysis and PPP together) of DINCH-, MINCH-, and rosiglitazone-treated cells compared to untreated control cells determined by labeling with [1,2-^{13}C]glucose. Values are expressed as mean ± SD (n = 4). Welch ANOVA followed by Games-Howell (A, B) and Dunnett's T3 (C, D) post-hoc test was performed to calculate statistical significance, and significant changes are displayed compared to the untreated control of the respective time point; *$p < 0.05$, **$p < 0.01$, ***$p < 0.001$. F1,6BP – fructose 1,6-bisphosphate, GM – glucose metabolism, G6P – glucose 6-phosphate, Gro3P – glycerol 3-phosphate, Lac ex. – lactate extracellular, PEP – phosphoenolpyruvate, Pyr – pyruvate, and Ru5P – ribulose 5-phosphate.

acetyl-CoA into the TCA cycle, this suggests an increased oxidative TCA cycle activity in rosiglitazone and 10 μM MINCH treatment. In contrast, while only minor changes in the labeling of TCA cycle metabolites were observed, the lower M+ 3 glutamate to M+ 5 glutamate ratio indicated a slightly decreased cycling through the TCA cycle at 24 h in 10 nM MINCH and DINCH treatment (Fig. 5C). Opposite to the oxidative TCA cycle flux, analysis of the M+ 5 citrate to the M+ 5 glutamate ratio after [U-^{13}C]glutamine incubation suggested significantly reduced reductive glutaminolysis activity in rosiglitazone-treated cells at 24 h, but no changes at 3 h and for the other treatments (Fig. 5D).

Besides the analysis of glutamine anaplerosis, pyruvate anaplerosis by pyruvate carboxylase was analyzed by subtracting the M+ 3 succinate from the M+ 3 aspartate to obtain the M+ 3 aspartate produced *via* pyruvate anaplerosis. In line with a reduced glucose labeling contribution, lower M+ 3 aspartate levels from M+ 3 pyruvate at 3 h were observed in rosiglitazone and 10 μM MINCH treatment, suggesting lower pyruvate carboxylase activity (Fig. 5E and Figure S10). Strikingly, this was reversed at 24 h with a trend towards higher M+ 3 aspartate levels from M+ 3 pyruvate in rosiglitazone treatment and even significantly increased levels after 10 μM MINCH treatment, which indicates an increase in the pyruvate carboxylase activity (Fig. 5E and Figure S10).

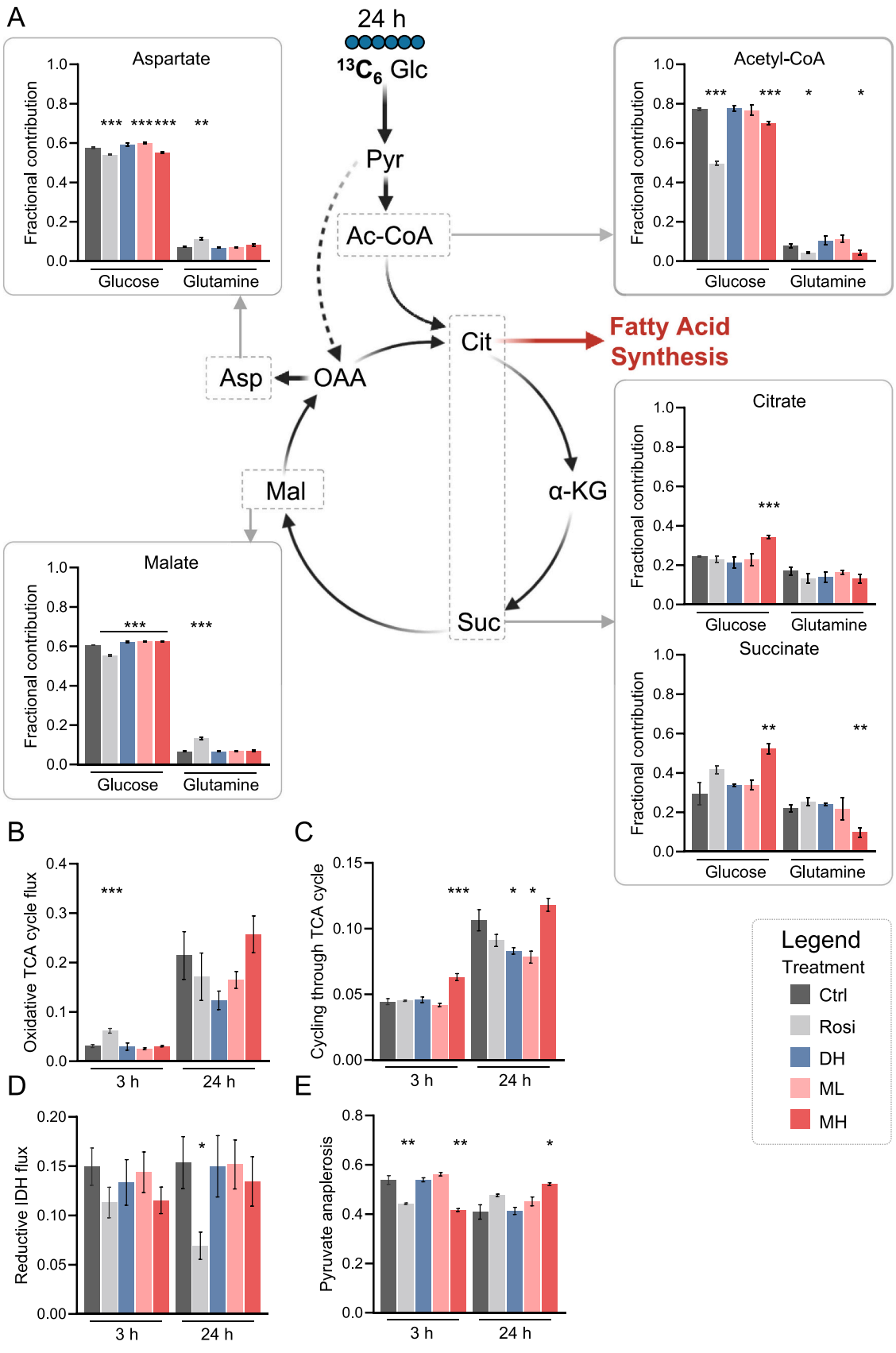

(caption on next page)

Fig. 5. Effects of DINCH and MINCH on acetyl-CoA metabolism and TCA cycle activity of treated mature adipocytes. (A) ^{13}C fractional contribution from glucose and glutamine to selected metabolites of the TCA cycle and acetyl-CoA of DINCH- and MINCH-treated mature SGBS adipocytes (DH – DINCH High (10 μM), ML – MINCH Low (10 nM), and MH – MINCH High (10 μM)), SGBS cells treated with rosiglitazone (Rosi) and untreated control cells (Ctrl) 24 h after labeling with [U-^{13}C]glucose and [U-^{13}C]glutamine on day 20, respectively. (B) Oxidative TCA cycle flux of DINCH-, MINCH-, and rosiglitazone-treated cells compared to untreated control cells after labeling with [U-^{13}C]glutamine, determined by the ratio of the M+ 4 isotopologue of citrate to the M+ 5 isotopologue of glutamate (C) Cycling of glutamate through the TCA cycle of DINCH-, MINCH-, and rosiglitazone-treated cells compared to untreated control cells, assessed after labeling with [U-^{13}C]glutamine by the ratio of the M+ 3 isotopologue of glutamate to the M+ 5 isotopologue of glutamate. (D) Reductive isocitrate dehydrogenase (IDH) flux of DINCH-, MINCH-, and rosiglitazone-treated cells compared to untreated control cells, assessed after labeling with [U-^{13}C]glutamine by the ratio of the M+ 3 isotopologue of citrate to the M+ 5 isotopologue of glutamate. (E) Pyruvate anaplerosis of DINCH-, MINCH-, and rosiglitazone-treated, as well as untreated control cells, after labeling with [U-^{13}C]glucose, determined by subtracting the M+ 3 isotopologue of succinate from the M+ 3 isotopologue of aspartate (surrogate for oxaloacetate). Values are expressed as mean ± SD (n = 4). Welch ANOVA followed by Games-Howell (A) and Dunnett's T3 (B, C, D, E) post-hoc test was performed to calculate statistical significance, and significant changes are shown compared to the untreated control; *$p < 0.05$, **$p < 0.01$, ***$p < 0.001$. Ac-CoA – acetyl coenzyme A, Asp – aspartate, Cit – citrate, Gln – glutamine, Glu – glutamate, α-KG – α-ketoglutarate, Mal – malate, OAA – oxaloacetate, Pyr – pyruvate, and Suc – succinate.

3.6. MINCH induces browning of mature adipocytes similar to rosiglitazone

Previous studies have shown that treatment of mature human white adipocytes with rosiglitazone induces a white-to-brite conversion (browning) characterized by upregulation of a metabolic futile cycle with enhanced lipolysis and fatty acid oxidation, as well as re-esterification at the same time [71,72]. Although a browning potential of SGBS cells was observed by differentiation of SGBS preadipocytes with rosiglitazone [73,74], potential browning after treatment of mature SGBS adipocytes has not been described so far. Thus, we investigated a potential browning effect after rosiglitazone treatment by analyzing the expression of brown/brite adipocyte markers and selected metabolic genes, and assessed whether similar changes can be induced by MINCH treatment, given the observed comparable metabolic changes. To ensure comparability with the ^{13}C metabolic tracing experiments, differentiated SGBS adipocytes were exposed under identical conditions as described above from day 12 to day 20, followed by incubation with conditioned medium without ^{13}C tracer for 24 h.

Phenotypically, like classical brown adipocytes, brite adipocytes are characterized by multilocular, small lipid droplets [22]. Interestingly, a 1.8- and 1.3-fold reduction in lipid droplet area was observed after 8 days of treatment and an additional 24 h incubation with conditioned DMEM/F12 without ^{13}C label in rosiglitazone and 10 μM MINCH-treated mature adipocytes, respectively (Fig. 6A and Figure S7). As expected from the absence of metabolic changes, no effects on the lipid droplet area were observed by 10 nM MINCH and DINCH treatment (Fig. 6A and Figure S7). To further characterize potential browning by rosiglitazone and 10 μM MINCH treatment, uncoupling protein 1 (UCP1) expression, which facilitates thermogenesis in brown and brite adipocytes [75], was analyzed 24 h after incubation with conditioned DMEM/F12 without ^{13}C label on day 20. As expected, a 28-fold increase in UCP1 expression was observed after rosiglitazone treatment and, interestingly, a 5-fold increase after 10 μM MINCH treatment (Fig. 6B). Analysis of UCP1 protein levels confirmed the substantial expression in rosiglitazone- and 10 μM MINCH-treated mature adipocytes compared to barely detectable levels in controls (Fig. 6C and D and Figure S12A). Assessment of the functional consequence of increased UCP1 expression by measuring the mitochondrial oxygen consumption rate (OCR) on day 20 revealed significantly increased basal respiration in rosiglitazone- and 10 μM MINCH-treated mature adipocytes (Fig. 6E and Figure S12B). Both treatments showed elevated ATP-coupled respiration, and MINCH-treated cells displayed significantly increased proton leak (uncoupled respiration), whereas rosiglitazone-treated cells showed only a trend towards increased proton leak (Fig. 6E and Figure S12B). No changes in maximal respiration or spare respiratory capacity were observed (Figure S12B and C).

Further analysis of brown/brite adipocyte markers showed elevated levels of the fatty acid transporter 3 (FABP3) and the insulin-sensitizing adipokine adiponectin (ADIPOQ) in rosiglitazone and 10 μM MINCH-treated cells (Figure S12D). In contrast, no induction of the brite/brown adipocyte markers PR domain containing 16 (PRDM16) and PPARG coactivator 1-alpha (PGC1α) was observed, but even a 2-fold decrease in PRDM16 expression in rosiglitazone and a slight decrease in PGC1α in rosiglitazone and 10 μM MINCH treatment (Figure S12D). Similarly, reduced PPARγ levels were observed in rosiglitazone and 10 μM MINCH-treated cells (Figure S12).

In addition to the brown/brite adipocyte markers, the expression of metabolic genes from fatty acid synthesis, lipolysis, and oxidative phosphorylation, described to be induced during white-to-brown conversion [71], was analyzed. Fatty acid synthase, a key enzyme of fatty acid synthesis, showed reduced expression in rosiglitazone and 10 μM MINCH-treated cells (Figure S12D). In contrast, analysis of the hormone-sensitive lipase (HSL), which is a pivotal enzyme of lipolysis, showed increased protein levels in rosiglitazone treatment, as well as induced protein levels of its phosphorylated, activated form pHSL in rosiglitazone and 10 μM MINCH treatment (Fig. 6F and Figure S12A). Protein levels of the complexes of oxidative phosphorylation showed slightly increased levels of complex II in rosiglitazone and 10 μM MINCH-treated cells, but no changes in the abundances of the other complexes (Fig. 6G and H and Figure S12E).

4. Discussion

Although no obesogenic effects of DINCH have been observed in application studies *in vivo* [47], the primary metabolite MINCH has been shown to promote adipocyte differentiation in rat and human preadipocytes [42,43]. In addition, the treatment of mature human adipocytes with DINCH and MINCH affected their function by inducing oxidative stress, altering adipokine secretion, and decreasing lipid content [42]. Induction of an altered adipocyte state by DINCH treatment was supported by a recent *in vivo* study in DINCH-exposed C57BL/6 N mice, in which no weight-promoting effects were observed in line with application studies, but an increase in the adipocyte size in visceral adipose tissue and changes in the expression of proteins in adipose tissue related to energy metabolism [48]. Since there is still limited data on the metabolic effects of DINCH and MINCH on adipocytes, we assessed changes in the metabolic pathway activity of treated human preadipocytes and mature adipocytes using ^{13}C metabolic tracing as a novel method for the identification of metabolism-disrupting properties.

Concentration analysis prior to metabolic assessment confirmed the intracellular uptake of DINCH and MINCH in mature adipocytes (Fig. 1), which we previously described in preadipocytes [57]. Comparison of the intracellular concentrations of MINCH revealed 1.4- to 3.7-fold higher concentrations in treated mature adipocytes compared to treated preadipocytes, despite the 4-day shorter treatment period. Since the log K_{ow} of MINCH is 5.2 [76], indicating high lipophilicity, we suggest that the higher intracellular concentrations can be attributed to the higher lipid content in mature adipocytes, comparable to the observed dependence of the intracellular concentrations of chlorinated paraffins on the cellular lipid content in 3T3-L1 adipocytes [77]. Although DINCH is more hydrophilic (log K_{ow}: 9.8 [76]) than MINCH, intracellular concentrations in mature adipocytes were slightly lower compared to previously measured levels in preadipocytes. This difference suggests a

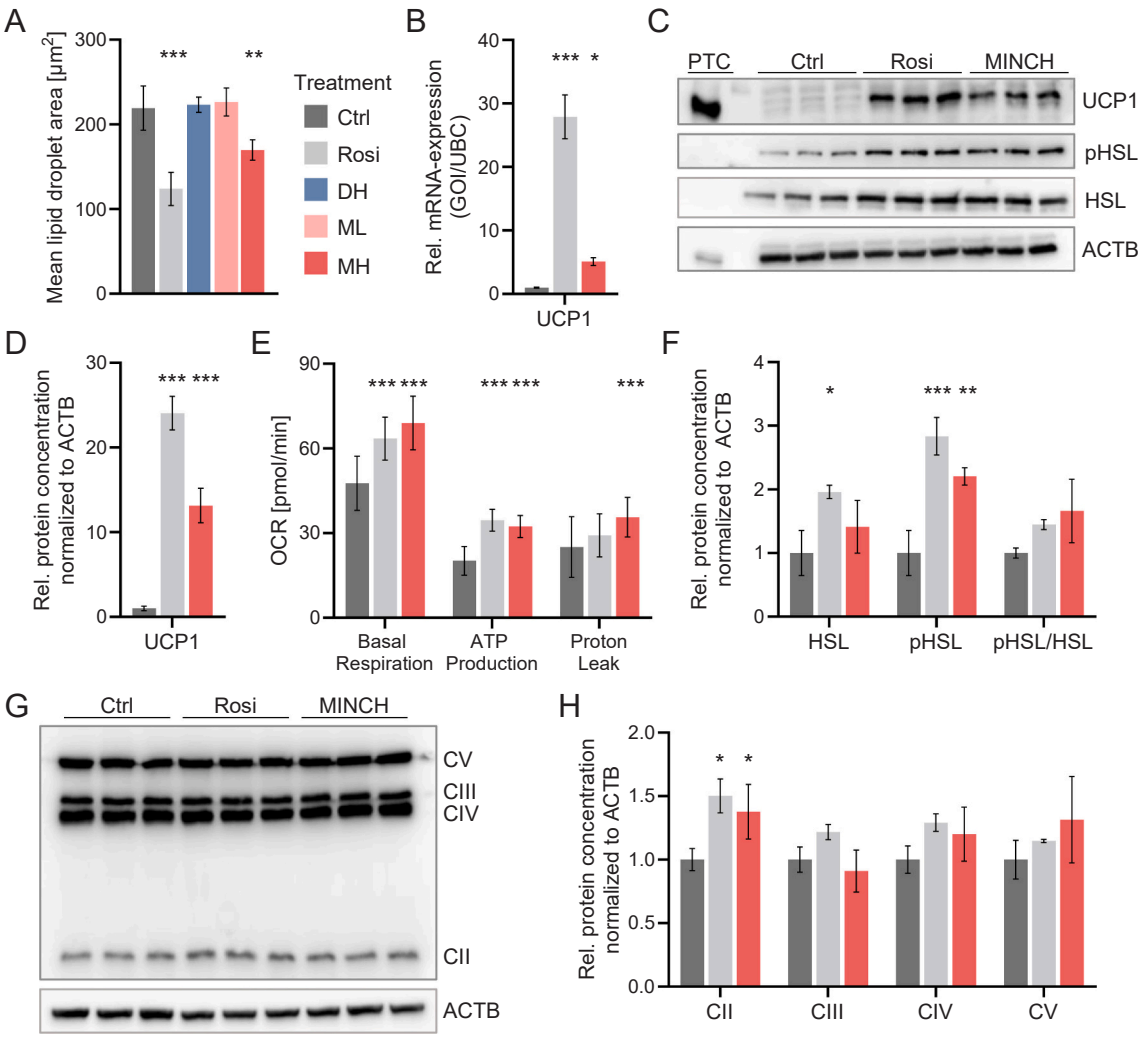

Fig. 6. Browning effects of MINCH in treated mature adipocytes. (A) Lipid droplet area of DINCH- and MINCH-treated mature SGBS adipocytes (ML – MINCH Low (10 nM) and MH – MINCH High (10 µM)), SGBS cells treated with rosiglitazone (Rosi), and untreated control cells 24 h after incubation with conditioned DMEM/F12 without ^{13}C label on day 20 (n = 4). (B) mRNA expression of UCP1 in 10 µM MINCH-treated and rosiglitazone-treated cells relative to the expression in untreated control cells 24 h after incubation with conditioned DMEM/F12 without ^{13}C label on day 20, calculated by the ΔΔCT method and normalized to ubiquitin C (UBC) expression (n = 4); GOI – gene of interest. (C) Western blot analysis of uncoupling protein 1 (UCP1), Ser660 phosphorylated HSL (pHSL) and hormone-sensitive lipase (HSL), in 10 µM MINCH-treated, rosiglitazone-treated, and untreated control cells 24 h after incubation with conditioned DMEM/F12 without ^{13}C label on day 20 (n = 3). A brown adipose tissue lysate was used as the positive control (PTC) for controlling the UCP1 lane. (D) Protein concentration of UCP1 in 10 µM MINCH-treated and rosiglitazone-treated cells relative to the concentration in untreated control cells 24 h after incubation with conditioned DMEM/F12 without ^{13}C label determined by immunoblotting and densitometric quantification (n = 3). (E) Basal respiration, ATP-coupled respiration and proton leak (uncoupled respiration) calculated based on the measurement of the oxygen consumption rate (OCR) in 10 µM MINCH-treated, rosiglitazone-treated and untreated control cells on day 20 (n = 18–20).(F) Protein concentrations of hormone-sensitive lipase (HSL) and Ser660 phosphorylated HSL (p-HSL), as well as the ratio of HSL to p-HSL, in 10 µM MINCH-treated and rosiglitazone-treated cells relative to the concentrations and the ratio in untreated control cells 24 h after incubation with conditioned DMEM/F12 without ^{13}C label on day 20, determined by immunoblotting and densitometric quantification (n = 3). (G) Western blot analysis of the complexes II-V of oxidative phosphorylation (SDHB, UQCRC2, MTCO1, and ATP5F1A) in 10 µM MINCH-treated, rosiglitazone-treated and untreated control cells 24 h after incubation with conditioned DMEM/F12 without ^{13}C label on day 20 (n = 3). (H) Protein concentrations of the enzyme complexes II-V of oxidative phosphorylation (SDHB, UQCRC2, MTCO1, and ATP5F1A) in 10 µM MINCH-treated and rosiglitazone-treated cells relative to the concentrations in the untreated control cells 24 h after incubation with conditioned DMEM/F12 without ^{13}C label on day 20, determined by immunoblotting and densitometric quantification (n = 3). Protein concentrations were normalized to β-actin (ACTB) values. CII – complex II: succinate dehydrogenase [ubiquinone] iron-sulfur subunit (SDHB), CIII – complex III: cytochrome b-c1 complex subunit 2 (UGCRC2), CIV – complex IV: cytochrome c oxidase subunit 1 (MTCO1), CV – complex V: ATP synthase subunit alpha (ATP5F1A). Values are expressed as mean ± SD. One-way ANOVA followed by Dunnett's post–hoc test against the untreated control was performed to calculate statistical significance, and significant changes are shown compared to the untreated control; *p < 0.05, **p < 0.01, ***p < 0.001.

greater influence of additional factors, such as stronger adsorption to the plastic surfaces, increased binding to medium proteins (e.g., transferrin), or enhanced biotransformation [78]. Indeed, we observed approximately a 2-fold higher conversion of DINCH to MINCH in mature adipocytes, but still at a rate of approximately pmol/10⁶cell/h, which is too low to account for the observed concentration differences. Notably, mature SGBS adipocytes also exhibited greater extra- and intracellular conversion of MINCH to OH-MINCH, as well as a conversion to oxo-MINCH that was not detected in preadipocytes. This indicates an overall higher biotransformation capacity (Fig. 1). These observations are consistent with the increased expression of biotransformation enzymes, including lipases and cytochromes P450, upon differentiation of SGBS cells [79,80]. Differences in intracellular concentrations and biotransformation capacity between preadipocytes and mature

adipocytes highlight the importance of concentration analysis when comparing different cell types and differentiation states [81].

After confirming intracellular uptake, we applied labeling with [U-^{13}C]glucose, [1,2-^{13}C]glucose, and [U-^{13}C]glutamine tracers to measure changes in the activity of central carbon metabolism in MINCH-treated preadipocytes (Figs. 2 and 3). Consistent with our previous results at the metabolite level, preadipocytes treated with 10 μM MINCH showed a similar metabolic response to rosiglitazone-differentiated cells at the pathway level. Together with the induction of lipid accumulation, metabolic pathway activity was rewired towards energy production and lipogenesis, including elevated glycolysis and PPP activity as well as increased production of the fatty acid precursors acetyl-CoA from glycolysis and reductive glutaminolysis. Furthermore, increased glucose contribution to the TCA cycle and upregulated pyruvate carboxylase activity for replenishment of the TCA cycle were observed in 10 μM MINCH and rosiglitazone treatment. These changes are consistent with previous studies, which assessed metabolic flux during adipogenesis of 3T3-L1 cells and observed increased flux through core metabolic pathways and identified strongly elevated pyruvate carboxylase flux as a key driver for *de novo* lipogenesis and adipogenesis [82–84]. In addition to the upregulated pyruvate carboxylase activity, transiently decreased oxidative TCA flux and decreased cycling of metabolites through the TCA cycle in 10 μM MINCH and rosiglitazone treatment indicate a switch of TCA metabolism towards providing building blocks for lipid production, instead of delivering NADH for energy production. Similarly, Oates and Antoniewicz reported reduced NADH generation from the TCA cycle upon differentiation, but instead increased contribution from glycolysis [82]. In contrast to the effects at μM concentrations, 10 nM MINCH treatment did not show induction of lipid accumulation and increased metabolite levels of the central carbon metabolism, similar to previous results [42,57]. However, ^{13}C metabolic tracing revealed an increase in glucose labeling of extracellular lactate, acetyl-CoA, and malate, suggesting a slight upregulation of glucose contribution to lactate and acetyl-CoA production, as well as higher pyruvate carboxylase activity. This resembles the changes observed at higher concentrations and indicate that even at nanomolar levels of MINCH, subtle metabolic alterations can be detected in human SGBS preadipocytes.

Beyond adipogenesis, the effect of MINCH on mature adipocytes, reflecting the potential effects on preexisting adipose tissue, was analyzed and responses were again compared to the PPARγ agonist rosiglitazone. Investigating metabolism-disrupting properties in mature adipocytes is particularly relevant, as they serve as the primary site of lipid storage and insulin responsiveness in adipose tissue, and metabolic impairments can affect whole-body energy homeostasis [14,85]. Phenotypically, the observed reduced lipid droplet size upon rosiglitazone treatment suggested an induction of browning of mature SGBS cells (Fig. 6), which has already been observed upon differentiation of SGBS preadipocytes with rosiglitazone [73,74]. Indeed, the browning effect of rosiglitazone was confirmed by the elevated expression and protein levels of UCP1 and increased expression of FABP3, essential for fatty acid oxidation in brown adipocytes [86], as well as adiponectin, recently associated with browning of white adipocytes [87]. Remarkably, similar changes, including substantial expression of UCP1 protein, indicate induction of browning in mature adipocytes also by treatment with 10 μM MINCH, but not by treatment with 10 nM MINCH or the parent compound DINCH (Fig. 6). Measurement of the mitochondrial OCR confirmed increased uncoupled respiration in MINCH-treated mature adipocytes, supporting a functional browning phenotype (Fig. 6). Similarly, rosiglitazone treatment showed a trend toward increased uncoupled respiration, indicating a mild activation of thermogenic mitochondrial function. The increase in ATP-coupled respiration in both treatments suggests enhanced cellular energy turnover and metabolic activity. In contrast to FABP3 and adiponectin, expression of the transcriptional regulators PRDM16 and PGC1α, important mediators in brite adipocyte development [88], was not induced, but was even reduced in rosiglitazone and 10 μM MINCH treatment. We hypothesize that this might be due to a negative feedback mechanism, similar to the reduced PPARG mRNA levels observed here and in the study by Barquissau et al., where the rosiglitazone-induced white-to-brite conversion of human multipotent adipose-derived stem cells (hASC) was analyzed [72].

Analysis of changes in pathway activity by ^{13}C metabolic tracing supports the observed browning effect of rosiglitazone and 10 μM MINCH treatment at the metabolic level (Figs. 4 and 5). Apart from upregulated glycolysis, which has been reported to be induced upon browning of mature 3T3-L1 cells [89], [U-^{13}C]glutamine labeling revealed elevated glyceroneogenesis flux for glycerol 3-phosphate (Gro3P) production in rosiglitazone and 10 μM MINCH treatment. As a precursor for triglyceride synthesis, Gro3P plays an essential role in brown adipose tissue by controlling the amount of fatty acids available for thermogenesis [90], and upregulated glyceroneogenesis, promoting triglyceride synthesis, has been observed upon browning of human adipocytes [72]. Apart from re-esterification, elevated synthesis of fatty acids by increased expression of fatty acid synthase (FASN) has been reported in human white adipose tissue upon rosiglitazone-induced browning [71]. On the contrary, we did not observe induction of FASN expression, but decreased levels after rosiglitazone and 10 μM MINCH treatment and 24 h of additional incubation with conditioned DMEM/F12 without ^{13}C label. Our results are, however, in line with Barquissau et al. [72], who did not observe changes in FASN expression after 4 days of rosiglitazone treatment of hASC and no increase, but rather a slight decrease in *de novo* lipogenesis rate measured after insulin stimulation.

Metabolically opposite to the synthesis of triglycerides, elevated lipolysis and increased β-oxidation of fatty acids have been reported upon rosiglitazone-induced browning of white adipocytes for fueling the TCA cycle and oxidative phosphorylation and ultimately thermogenesis [71,72]. In line with this observation, we measured elevated levels of the phosphorylated hormone-sensitive lipase and decreased triglyceride content, which indicate upregulation of lipolysis in rosiglitazone and 10 μM MINCH treatment. Together with the increased lipolysis, the observed source switch for acetyl-CoA synthesis by strongly decreased acetyl-CoA labeling from glucose and glutamine suggests increased β-oxidation of fatty acids in rosiglitazone and 10 μM MINCH treatment. These changes were accompanied by a higher flux of acetyl-CoA in the TCA cycle, which, along with transiently upregulated oxidative TCA cycle flux and cycling of metabolites through the TCA cycle, indicates an overall increase in oxidative TCA cycle activity. This higher oxidative capacity in rosiglitazone and 10 μM MINCH treatment was confirmed by increased protein levels of succinate dehydrogenase, which is involved in both the TCA cycle and complex II of oxidative phosphorylation and has been identified as an important mediator in the activation of brown adipose tissue thermogenesis [91]. Similar to previous results [92,93], we observed increased pyruvate anaplerosis *via* pyruvate carboxylase flux, in addition to higher glutamine anaplerosis towards malate and oxaloacetate for maintenance of this increased oxidative TCA cycle flux. Overall, the increased lipolysis, fatty acid oxidation, and simultaneous re-esterification indicate upregulation of a triglyceride/fatty acid metabolic futile cycle in rosiglitazone and MINCH-treated cells, identified in brite/brown adipocytes besides UCP1-dependent thermogenesis as an important fine-tuning mechanism for non-shivering thermogenesis [71,94].

A previously performed proteomic analysis of mature SGBS adipocytes treated with MINCH, apart from upregulation of lipolysis, did not indicate induction of browning at the protein level but rather showed downregulation of proteins related to energy production, including the TCA cycle and oxidative phosphorylation [42]. Apart from differences in the experimental setup as we analyzed the metabolic changes following insulin stimulation, we hypothesize that this discrepancy between the lower protein levels in these pathways and our observed higher metabolic fluxes may be attributed to a regulation of pathway activity at post-translational level such as allosteric regulation [95] or differences

in the temporal dynamics between protein levels and metabolite fluxes [96]. In contrast, the observed browning in human adipocytes by MINCH treatment in this study is consistent with the results by Hsu et al., who observed a similar induction of browning by the primary metabolite of the phthalate DEHP, MEHP, in 3T3-L1 cells *in vitro* after treatment with μM concentrations and of white adipose tissue *in vivo* after treatment of C57BL/6 J with 1 mg/kg bw/d DEHP [27]. Although the induction of browning has been primarily associated with beneficial metabolic effects including improved insulin sensitivity and obesity resistance [97,98], adverse outcomes have also been reported, including contributions to hypermetabolism and associated cachexia in cancer [99], as well as hepatic steatosis after burn injury via pro-inflammatory fatty acid release [100]. Thus, further research is necessary to decipher the metabolic consequences of the induction of browning by MINCH and other environmental chemicals such as MEHP *in vivo* [23].

Previous studies suggest that the adipogenic effect of MINCH was mainly mediated *via* binding and activating PPARγ [42,46]. Similarly, we observed that the MINCH-induced metabolic changes were mainly similar to the changes induced by rosiglitazone in preadipocytes and mature adipocytes. Nevertheless, we observed subtle differences in the effects on metabolic pathway activity, including increased glycolysis contribution to glucose metabolism by MINCH treatment, whereas increased PPP contribution to glucose metabolism by rosiglitazone treatment was consistently observed in preadipocytes and mature adipocytes. This higher glycolytic activity seen after MINCH treatment might also explain further observed differences, such as the higher labeling contribution from [U-^{13}C]glucose in the TCA cycle metabolites from citrate to succinate in mature adipocytes. Apart from the possibility of different recruitment of transcription factors upon PPARγ activation by MINCH compared to rosiglitazone [101], our findings are consistent with the notion that MINCH exerts effects beyond canonical PPARγ-signaling. This interpretation aligns with our previous observation that metabolic effects of MINCH persisted in the presence of the PPARγ inhibitor GW9662 [57]. Moreover, Campioli et al. suggested PPARα as the main initiator of the MINCH-induced differentiation in adipocytes since effects were blocked by a PPARα antagonist and only partially by a PPARγ antagonist. This was a view further supported by the induction of PPARα activity by MINCH in a GAL4-UAS reporter gene assay [45].

Besides binding to other nuclear hormone receptors, there are also other potential candidates responsible for the PPARγ-independent effects by MINCH. A recently published thermal proteome profiling screening indicated indirect interactions of MINCH with extracellular signal-regulated kinase 1 (ERK1) and C-terminal c-Src kinase (CSK) during early adipogenesis in SGBS cells [102]. In line with this, phosphoproteome profiling revealed that MINCH induced a PPARγ-independent increase in the Y204 phosphorylation site of ERK1 required for its activation [102]. ERK1 and CSK have been implicated in glycolytic regulation in cancer cells, raising the possibility that their modulation contributes to the observed glycolytic effects of MINCH [103,104].

While these observations collectively point towards PPARγ-independent mechanisms, we acknowledge that direct experimental proof would be required. Specific test designed to test causality such as genetic knockdowns or inhibition of candidate kinases are beyond the scope of the presented study but represent an important direction for further validation.

Effects of MINCH on metabolic pathway activity in exposed preadipocytes and mature adipocytes were observed primarily at micromolar concentrations, consistent with previous *in vitro* studies [42,43,45]. Although serum concentrations of DINCH and its metabolites, which better approximate the concentrations in adipose tissue, are missing so far, current biomonitoring studies reported geometric mean concentrations of DINCH metabolites ranging from 2.5 to 3.6 μg/L in European children and adolescents [40] and median OH-MINCH concentrations of 0.8–1.1 μg/L in US children and adolescents [105]. These exposure levels are approximately three orders of magnitude lower than the concentrations at which pronounced effects on adipocyte metabolism were observed *in vitro*. Thus, the observed effects of MINCH are likely to be non-environmentally relevant. Nevertheless, it should be noted that under specific exposure scenarios, such as in intensive care unit (ICU) patients, micromolar serum concentrations of plasticizer metabolites have been reported for structurally related compounds like DEHP [63]. While comparable data for DINCH are lacking, these findings suggest that high exposure situations for the population cannot be entirely excluded. Additionally, potential bioaccumulation of DINCH in adipose tissue could represent a further factor enabling its primary metabolite MINCH to reach higher local concentrations *in vivo*. While application studies did not indicate relevant accumulation [47,106], elevated DINCH levels were detected in subcutaneous and visceral WAT of dietary exposed C57BL/6 N mice after a recovery phase [48], suggesting possible retention in adipose tissue. These contradictory findings highlight the need for further research into the bioaccumulation potential of DINCH and its implications for MINCH-mediated metabolism-disrupting effects.

Importantly, the detection of minor changes at nanomolar concentrations highlights the high sensitivity of the $^{1\,3}$C metabolic tracing approach. The biological relevance of these low-dose alterations remains uncertain but warrants further investigation, particularly in the context of chronic exposure or in combination with other environmental chemicals. Indeed, different mixtures of organic and inorganic contaminants have been shown to elicit synergistic adipogenic effects greater than those of the single compounds [107]. Such effects may be of particular concern for vulnerable populations like infants and children, given the increasing exposure trends of DINCH in these groups [40,108] and the developmental determination of adipocyte number during childhood [70]. Enhanced adipogenesis during this critical window may contribute to a permanently increased adipocyte number and a greater risk of obesity in adulthood [109,110]. Overall, our results highlight the utility of ^{13}C metabolic tracing in human adipocytes as a sensitive method for detecting adipogenic effects and subtle metabolic alterations upon treatment with environmental chemicals. In contrast to single-endpoint assays such as analysis of lipid accumulation [111], this approach offers higher sensitivity and, importantly, provides insights into the underlying molecular mode of action. Similar to $^{1\,3}$C metabolic tracing, transcriptomics and proteomics can be used to investigate molecular mechanisms and have been applied to assess metabolism-disrupting properties of chemicals, particularly adipogenesis-promoting effects [20,51,112,113]. For example, transcriptomics has been successfully used in 3T3-L1 cells to distinguish obesogens from non-obesogens [51] and to classify adipogenic chemicals according to their ability to induce a white or brite adipocyte phenotype [112]. Likewise, proteomics has confirmed the adipogenic potential of per- and polyfluoroalkyl substances in 3T3-L1 cells and revealed the underlying molecular regulation [113]. In human SGBS adipocytes, proteomics further identified a dysfunctional adipocyte state induced by BPA and its substitutes, characterized by increased inflammatory signaling and reduced insulin sensitivity [20]. While these studies demonstrate the usefulness of transcriptomics and proteomics for assessing metabolism-disrupting properties, a key advantage of $^{1\,3}$C metabolic tracing is that it is more directly linked to the phenotype [56,58,114]. By contrast, changes observed at the transcript or protein level do not necessarily translate into functional metabolic alterations [114]. Finally, unlike metabolomics, which provides static snapshots of metabolite abundances, ^{13}C metabolic tracing provides dynamic insights into metabolic fluxes and pathway activity [58], enabling a more mechanistic understanding of how MDCs interfere with cellular metabolism. Given the need for the development of new assessment strategies for testing metabolism-disrupting properties and the great potential of omics techniques for enhancing risk assessment [53], we propose ^{13}C metabolic tracing as a supplementary New Approach Methodology within the OECD test guideline framework.

5. Conclusion

Using ^{1} ^{3}C metabolic tracing, we demonstrated that MINCH, a primary metabolite of DINCH, alters key metabolic pathways in treated human preadipocytes and mature adipocytes (Fig. 7). In preadipocytes during differentiation, MINCH enhanced metabolic activity towards lipid synthesis, confirming its adipogenesis-promoting potential. In mature adipocytes, MINCH promoted a metabolic profile characteristic of browning. Effects partially mimicked the PPARγ agonist rosiglitazone but MINCH also induced distinct PPARγ-independent effects such as enhanced glycolysis.

Although changes in the metabolism of exposed preadipocytes and mature adipocytes were observed mainly at micromolar concentrations, which are several orders of magnitude above current human exposure estimates, ^{1} ^{3}C metabolic tracing also detected subtle metabolic changes at 10 nM MINCH in preadipocytes. While the biological significance of these low-dose findings remains unclear, they underscore the sensitivity of ^{1} ^{3}C metabolic tracing to detect early metabolic alterations caused by chemical exposure. Taken together, these results support the potential of this approach as a New Approach Methodology for evaluating metabolism-disrupting properties of environmental chemicals.

Environmental implication

Possible metabolism-disrupting properties of certain plasticizers and their ubiquitous occurrence might contribute to the worldwide increase in metabolic diseases. Since the metabolism-disrupting properties of the plasticizer DINCH remain controversial, further studies are needed to investigate whether and how DINCH and its metabolite MINCH affect adipocyte physiology at the molecular level. This study explored the effects of MINCH on human preadipocytes and mature adipocytes using ^{13}C metabolic tracing of central carbon metabolism as a novel method to detect disruptions of adipocyte metabolism. Subtle changes were already detectable at nM concentrations, but their biological relevance requires further investigations.

CRediT authorship contribution statement

Martin Wabitsch: Resources. **Alix Sarah Aldehoff:** Writing – review & editing, Investigation. **Kristin Schubert:** Writing – review & editing, Supervision. **John T Heiker:** Writing – review & editing, Supervision, Resources. **Matthias Blüher:** Writing – review & editing, Funding acquisition. **Martin von Bergen:** Writing – review & editing, Supervision, Funding acquisition. **Rolle-Kampczyk Ulrike Elisabeth:** Writing – review & editing, Supervision, Project administration, Conceptualization. **Cornelius Goerdeler:** Writing – original draft, Visualization, Validation, Methodology, Investigation, Data curation, Conceptualization. **Helen Broghammer:** Writing – review & editing, Methodology, Investigation. **Beatrice Engelmann:** Writing – original draft, Supervision, Methodology, Data curation, Conceptualization.

Funding

This research was funded by the German Research Foundation (Deutsche Forschungsgemeinschaft, DFG) through the CRC 1052 "Obesity Mechanisms", project number 209933838 (B1 MB and MvB, C7 JTH, Z3 MvB). BE and MvB are grateful for funding by the Novo Nordisk Foundation (grant NNF21OC0066551). KS is grateful for funding from

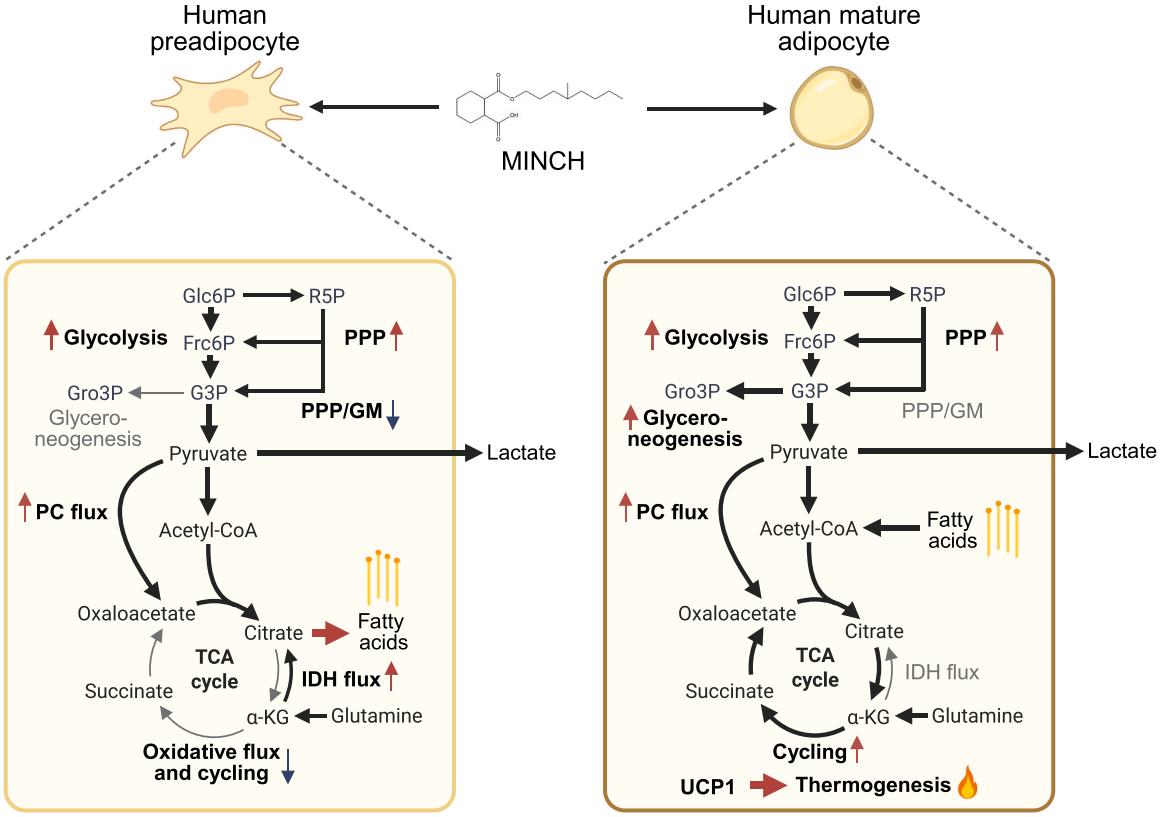

Fig. 7. Effects of MINCH on the metabolism of human preadipocytes during differentiation and mature adipocytes. In preadipocytes, MINCH exposure resulted in an upregulation of glycolysis and PPP and shifted TCA metabolism toward lipid synthesis by inducing upregulation of PC and IDH flux, thereby confirming its adipogenic effect. In mature adipocytes, MINCH induced glycolysis, glyceroneogenesis, fatty acid oxidation, and oxidative TCA cycle metabolism, demonstrating induction of browning together with increased UCP1 levels. Partly distinct metabolic effects of MINCH compared to the PPARγ agonist rosiglitazone, including higher glycolytic activity, confirm mediation, at least in part, *via* a PPARγ-independent mechanism. PC – pyruvate carboxylase, PPP/GM – contribution of the PPP to the glucose metabolism, IDH – isocitrate dehydrogenase (red arrows – elevated pathway activity; blue arrows – decreased pathway activity).

the German Research Foundation (project no. 530364326). MW was funded in part by the Federal Ministry of Education and Research (Bundesministerium für Bildung und Forschung, BMBF) as part of the German Center for Child and Adolescent Health (DZKJ) (01GL2407A). HB is supported by a fellowship of the Studienstiftung des deutschen Volkes.

Declaration of Competing Interest

MB received honoraria as a consultant and speaker from Amgen, Astra-Zeneca, Bayer, Boehringer-Ingelheim, Lilly, Novo Nordisk, Novartis, Pfizer, and Sanofi. All other authors declare no competing interests.

Acknowledgment

We thank Olivia Pleßow and Nicole Bock for their competent technical assistance with the LC-MS measurements and the sample preparation. We are grateful for the support of the NMDR/Metabolomics Workbench, which is supported by Metabolomics Workbench/National Metabolomics Data Repository (NMDR) (grant# U2C-DK119886), Common Fund Data Ecosystem (CFDE) (grant# 3OT2OD030544) and Metabolomics Consortium Coordinating Center (M3C) (grant# 1U2C-DK119889). The graphical abstract, Fig. 7, and Figure S1 were created in BioRender.

Appendix A. Supporting information

Supplementary data associated with this article can be found in the online version at doi:10.1016/j.jhazmat.2025.140384.

Data availability

The metabolome data of this study are available at the NIH Common Fund's National Metabolomics Data Repository (NMDR) website, the Metabolomics Workbench [115], where it has been assigned the project ID PR002515. The data can be accessed directly *via* its project DOI: https://doi.org/10.21228/M8JN9T.

References

[1] NCD Risk Factor Collaboration (NCD-RisC), 2024. Worldwide trends in underweight and obesity from 1990 to 2022: a pooled analysis of 3663 population-representative studies with 222 million children, adolescents, and adults. Lancet 403, 1027–1050. https://doi.org/10.1016/S0140-6736(23)02750-2.

[2] Okunogbe, A., Nugent, R., Spencer, G., Powis, J., Ralston, J., Wilding, J., 2022. Economic impacts of overweight and obesity: current and future estimates for 161 countries. BMJ Glob Health 7. https://doi.org/10.1136/bmjgh-2022-009773.

[3] Li, L., Liu, D.-W., Yan, H.-Y., Wang, Z.-Y., Zhao, S.-H., Wang, B., 2016. Obesity is an independent risk factor for non-alcoholic fatty liver disease: evidence from a meta-analysis of 21 cohort studies. Obes Rev 17, 510–519. https://doi.org/10.1111/obr.12407.

[4] Vazquez, G., Duval, S., Jacobs, D.R., Silventoinen, K., 2007. Comparison of body mass index, waist circumference, and waist/hip ratio in predicting incident diabetes: a meta-analysis. Epidemiol Rev 29, 115–128. https://doi.org/10.1093/epirev/mxm008.

[5] Stunkard, A.J., Harris, J.R., Pedersen, N.L., McClearn, G.E., 1990. The body-mass index of twins who have been reared apart. N Engl J Med 322, 1483–1487. https://doi.org/10.1056/NEJM199005243222102.

[6] Loos, R.J.F., Yeo, G.S.H., 2022. The genetics of obesity: from discovery to biology. Nat Rev Genet 23, 120–133. https://doi.org/10.1038/s41576-021-00414-z.

[7] Pietiläinen, K.H., Kaprio, J., Borg, P., Plasqui, G., Yki-Järvinen, H., Kujala, U.M., Rose, R.J., Westerterp, K.R., Rissanen, A., 2008. Physical inactivity and obesity: a vicious circle. Obes (Silver Spring Md) 16, 409–414. https://doi.org/10.1038/oby.2007.72.

[8] Fedde, S., Stolte, A., Plachta-Danielzik, S., Müller, M.J., Bosy-Westphal, A., 2024. Ultra-processed food consumption and overweight in children, adolescents and young adults: Long-term data from the Kiel Obesity Prevention Study (KOPS). Pediatr Obes, e13192. https://doi.org/10.1111/ijpo.13192.

[9] Hall, K.D., Ayuketah, A., Brychta, R., Cai, H., Cassimatis, T., Chen, K.Y., Chung, S. T., Costa, E., Courville, A., Darcey, V., Fletcher, L.A., Forde, C.G., Gharib, A.M., Guo, J., Howard, R., Joseph, P.V., McGehee, S., Ouwerkerk, R., Raisinger, K., Rozga, I., Stagliano, M., Walter, M., Walter, P.J., Yang, S., Zhou, M., 2019. Ultra-processed diets cause excess calorie intake and weight gain: an inpatient randomized controlled trial of ad libitum food intake. Cell Metab 30, 67–77.e3. https://doi.org/10.1016/j.cmet.2019.05.008.

[10] Biemann, R., Blüher, M., Isermann, B., 2021. Exposure to endocrine-disrupting compounds such as phthalates and bisphenol A is associated with an increased risk for obesity. Best Pract Res Cl En 35, 101546. https://doi.org/10.1016/j.beem.2021.101546.

[11] Chamorro-Garcia, R., Diaz-Castillo, C., Shoucri, B.M., Käch, H., Leavitt, R., Shioda, T., Blumberg, B., 2017. Ancestral perinatal obesogen exposure results in a transgenerational thrifty phenotype in mice. Nat Commun 8, 2012. https://doi.org/10.1038/s41467-017-01944-z.

[12] Liu, Y., Peterson, K.E., 2015. Maternal Exposure to Synthetic Chemicals and Obesity in the Offspring: Recent Findings. Curr Environ Health Rep 2, 339–347. https://doi.org/10.1007/s40572-015-0068-6.

[13] Heindel, J.J., Blumberg, B., Cave, M., Machtinger, R., Mantovani, A., Mendez, M. A., Nadal, A., Palanza, P., Panzica, G., Sargis, R., Vandenberg, L.N., vom Saal, F., 2017. Metabolism disrupting chemicals and metabolic disorders. Reprod Toxicol 68, 3–33. https://doi.org/10.1016/j.reprotox.2016.10.001.

[14] Rosen, E.D., Spiegelman, B.M., 2006. Adipocytes as regulators of energy balance and glucose homeostasis. Nature 444, 847–853. https://doi.org/10.1038/nature05483.

[15] La Merrill, M.A., Smith, M.T., McHale, C.M., Heindel, J.J., Atlas, E., Cave, M.C., Collier, D., Guyton, K.Z., Koliwad, S., Nadal, A., Rhodes, C.J., Sargis, R.M., Zeise, L., Blumberg, B., 2025. Consensus on the key characteristics of metabolism disruptors. Nat Rev Endocrinol 21, 245–261. https://doi.org/10.1038/s41574-024-01059-8.

[16] Grün, F., Watanabe, H., Zamanian, Z., Maeda, L., Arima, K., Cubacha, R., Gardiner, D.M., Kanno, J., Iguchi, T., Blumberg, B., 2006. Endocrine-disrupting organotin compounds are potent inducers of adipogenesis in vertebrates. Mol Endocrinol 20, 2141–2155. https://doi.org/10.1210/me.2005-0367.

[17] Ariemma, F., D'Esposito, V., Liguoro, D., Oriente, F., Cabaro, S., Liotti, A., Cimmino, I., Longo, M., Beguinot, F., Formisano, P., Valentino, R., 2016. Low-Dose Bisphenol-A Impairs Adipogenesis and Generates Dysfunctional 3T3-L1 Adipocytes. PLOS ONE 11, e0150762. https://doi.org/10.1371/journal.pone.0150762.

[18] Ahn, Y.-A., Baek, H., Choi, M., Park, J., Son, S.J., Seo, H.J., Jung, J., Seong, J.K., Lee, J., Kim, S., 2020. Adipogenic effects of prenatal exposure to bisphenol S (BPS) in adult F1 male mice. Sci Total Environ 728, 138759. https://doi.org/10.1016/j.scitotenv.2020.138759.

[19] Shoucri, B.M., Hung, V.T., Chamorro-García, R., Shioda, T., Blumberg, B., 2018. Retinoid X receptor activation during adipogenesis of female mesenchymal stem cells programs a dysfunctional adipocyte. Endocrinology 159, 2863–2883. https://doi.org/10.1210/en.2018-00056.

[20] Schaffert, A., Krieg, L., Weiner, J., Schlichting, R., Ueberham, E., Karkossa, I., Bauer, M., Landgraf, K., Junge, K.M., Wabitsch, M., Lehmann, J., Escher, B.I., Zenclussen, A.C., Körner, A., Blüher, M., Heiker, J.T., von Bergen, M., Schubert, K., 2021. Alternatives for the worse: molecular insights into adverse effects of bisphenol a and substitutes during human adipocyte differentiation. Environ Int 156, 106730. https://doi.org/10.1016/j.envint.2021.106730.

[21] Zhang, W., Gao, Y., Chen, C., Li, A., Ma, X., Liang, Y., Yao, X., Song, M., Jiang, G., 2021. Bisphenol S Promotes the Formation of Visceral Fat in Mice. Environ Sci Technol Lett 8, 699–704. https://doi.org/10.1021/acs.estlett.1c00419.

[22] Giralt, M., Villarroya, F., 2013. White, brown, beige/brite: different adipose cells for different functions? Endocrinology 154, 2992–3000. https://doi.org/10.1210/en.2013-1403.

[23] Francis, C.E., Allee, L., Nguyen, H., Grindstaff, R.D., Miller, C.N., Rayalam, S., 2021. Endocrine disrupting chemicals: Friend or foe to brown and beige adipose tissue? Toxicology 463, 152972. https://doi.org/10.1016/j.tox.2021.152972.

[24] Wen, X., Xiao, Y., Xiao, H., Tan, X., Wu, B., Li, Z., Wang, R., Xu, X., Li, T., 2023. Bisphenol S induces brown adipose tissue whitening and aggravates diet-induced obesity in an estrogen-dependent manner. Cell Rep 42, 113504. https://doi.org/10.1016/j.celrep.2023.113504.

[25] Graceli, J.B., da Costa, C.S., Laws, M.J., Deviney, A.R.K., Meling, D., Flaws, J.A., 2023. Chronic exposure to a mixture of phthalates shifts the white and brown adipose tissue phenotypes in female mice. Toxicol Sci 193, 204–218. https://doi.org/10.1093/toxsci/kfad032.

[26] van Esterik, J.C.J., Dollé, M.E.T., Lamoree, M.H., van Leeuwen, S.P.J., Hamers, T., Legler, J., van der Ven, L.T.M., 2014. Programming of metabolic effects in C57BL/6JxFVB mice by exposure to bisphenol A during gestation and lactation. Toxicology 321, 40–52. https://doi.org/10.1016/j.tox.2014.04.001.

[27] Hsu, J.-W., Nien, C.-Y., Yeh, S.-C., Tsai, F.-Y., Chen, H.-W., Lee, T.-S., Chen, S.-L., Kao, Y.-H., Tsou, T.-C., 2020. Phthalate exposure causes browning-like effects on adipocytes in vitro and in vivo. Food Chem Toxicol 142, 111487. https://doi.org/10.1016/j.fct.2020.111487.

[28] Geyer, R., Jambeck, J.R., Law, K.L., 2017. Production, use, and fate of all plastics ever made. Sci Adv 3, e1700782. https://doi.org/10.1126/sciadv.1700782.

[29] Bui, T.T., Giovanoulis, G., Cousins, A.P., Magnér, J., Cousins, I.T., de Wit, C.A., 2016. Human exposure, hazard and risk of alternative plasticizers to phthalate esters. Sci Total Environ 541, 451–467. https://doi.org/10.1016/j.scitotenv.2015.09.036.

[30] M. Holland, Socio-economic assessment of phthalates, OECD Environment Working Papers, 133rd ed., 2018.

[31] Wassenaar, P.N.H., Legler, J., 2017. Systematic review and meta-analysis of early life exposure to di(2-ethylhexyl) phthalate and obesity related outcomes in

rodents. Chemosphere 188, 174–181. https://doi.org/10.1016/j.chemosphere.2017.08.165.
[32] Ribeiro, C.M., Beserra, B.T.S., Silva, N.G., Lima, C.L., Rocha, P.R.S., Coelho, M.S., Neves, F.D.A.R., Amato, A.A., 2020. Exposure to endocrine-disrupting chemicals and anthropometric measures of obesity: a systematic review and meta-analysis. BMJ Open 10, e033509. https://doi.org/10.1136/bmjopen-2019-033509.
[33] Feige, J.N., Gelman, L., Rossi, D., Zoete, V., Métivier, R., Tudor, C., Anghel, S.I., Grosdidier, A., Lathion, C., Engelborghs, Y., Michielin, O., Wahli, W., Desvergne, B., 2007. The endocrine disruptor monoethyl-hexyl-phthalate is a selective peroxisome proliferator-activated receptor gamma modulator that promotes adipogenesis. J Biol Chem 282, 19152–19166. https://doi.org/10.1074/jbc.M702724200.
[34] Biemann, R., Navarrete Santos, A., Navarrete Santos, A., Riemann, D., Knelangen, J., Blüher, M., Koch, H., Fischer, B., 2012. Endocrine disrupting chemicals affect the adipogenic differentiation of mesenchymal stem cells in distinct ontogenetic windows. Biochem Biophys Res Co 417, 747–752. https://doi.org/10.1016/j.bbrc.2011.12.028.
[35] Klöting, N., Hesselbarth, N., Gericke, M., Kunath, A., Biemann, R., Chakaroun, R., Kosacka, J., Kovacs, P., Kern, M., Stumvoll, M., Fischer, B., Rolle-Kampczyk, U., Feltens, R., Otto, W., Wissenbach, D.K., von Bergen, M., Blüher, M., 2015. Di-(2-Ethylhexyl)-Phthalate (DEHP) Causes Impaired Adipocyte Function and Alters Serum Metabolites. PLOS ONE 10, e0143190. https://doi.org/10.1371/journal.pone.0143190.
[36] Hao, C., Cheng, X., Xia, H., Ma, X., 2012. The endocrine disruptor mono-(2-ethylhexyl) phthalate promotes adipocyte differentiation and induces obesity in mice. Biosci Rep 32, 619–629. https://doi.org/10.1042/BSR20120042.
[37] Schmidt, J.-S., Schaedlich, K., Fiandanese, N., Pocar, P., Fischer, B., 2012. Effects of di(2-ethylhexyl) phthalate (DEHP) on female fertility and adipogenesis in C3H/N mice. Environ Health Persp 120, 1123–1129. https://doi.org/10.1289/ehp.1104016.
[38] EU Commission, 1999/815/EC: Commission Decision of 7 December 1999 adopting measures prohibiting the placing on the market of toys and childcare articles intended to be placed in the mouth by children under three years of age made of soft PVC containing one or more of the substances di-iso-nonyl phthalate (DINP), di(2-ethylhexyl) phthalate (DEHP), dibutyl phthalate (DBP), di-iso-decyl phthalate (DIDP), di-n-octyl phthalate (DNOP), and butylbenzyl phthalate (BBP), 1999.
[39] U.S. Congress., Consumer Product Safety Improvement Act of 2008., 2008.
[40] Vogel, N., Schmidt, P., Lange, R., Gerofke, A., Sakhi, A.K., Haug, L.S., Jensen, T. K., Frederiksen, H., Szigeti, T., Csákó, Z., Murinova, L.P., Sidlovska, M., Janasik, B., Wasowicz, W., Tratnik, J.S., Mazej, D., Gabriel, C., Karakitsios, S., Barbone, F., Rosolen, V., Rambaud, L., Riou, M., Murawski, A., Leseman, D., Koppen, G., Covaci, A., Lignell, S., Lindroos, A.K., Zvonar, M., Andryskova, L., Fabelova, L., Richterova, D., Horvat, M., Kosjek, T., Sarigiannis, D., Maroulis, M., Pedraza-Diaz, S., Cañas, A., Verheyen, V.J., Bastiaensen, M., Gilles, L., Schoeters, G., Esteban-López, M., Castaño, A., Govarts, E., Koch, H.M., Kolossa-Gehring, M., 2023. Current exposure to phthalates and DINCH in European children and adolescents - Results from the HBM4EU Aligned Studies 2014–2021. Int J Hyg Environ 249, 114101. https://doi.org/10.1016/j.ijheh.2022.114101.
[41] Harmon, P., Otter, R., 2022. A review of common non-ortho-phthalate plasticizers for use in food contact materials. Food Chem Toxicol 164, 112984. https://doi.org/10.1016/j.fct.2022.112984.
[42] Schaffert, A., Karkossa, I., Ueberham, E., Schlichting, R., Walter, K., Arnold, J., Blüher, M., Heiker, J.T., Lehmann, J., Wabitsch, M., Escher, B.I., von Bergen, M., Schubert, K., 2022. Di-(2-ethylhexyl) phthalate substitutes accelerate human adipogenesis through PPARγ activation and cause oxidative stress and impaired metabolic homeostasis in mature adipocytes. Environ Int 164, 107279. https://doi.org/10.1016/j.envint.2022.107279.
[43] Campioli, E., Duong, T.B., Deschamps, F., Papadopoulos, V., 2015. Cyclohexane-1,2-dicarboxylic acid diisononyl ester and metabolite effects on rat epididymal stromal vascular fraction differentiation of adipose tissue. Environ Res 140, 145–156. https://doi.org/10.1016/j.envres.2015.03.036.
[44] Kratochvil, I., Hofmann, T., Rother, S., Schlichting, R., Moretti, R., Scharnweber, D., Hintze, V., Escher, B.I., Meiler, J., Kalkhof, S., von Bergen, M., 2019. Mono(2-ethylhexyl) phthalate (MEHP) and mono(2-ethyl-5-oxohexyl) phthalate (MEOHP) but not di(2-ethylhexyl) phthalate (DEHP) bind productively to the peroxisome proliferator-activated receptor γ. Rapid Commun Mass Sp 33 1, 75–85. https://doi.org/10.1002/rcm.8258.
[45] Engel, A., Buhrke, T., Kasper, S., Behr, A.-C., Braeuning, A., Jessel, S., Seidel, A., Völkel, W., Lampen, A., 2018. The urinary metabolites of DINCH® have an impact on the activities of the human nuclear receptors ERα, ERβ, AR, PPARα and PPARγ. Toxicol Lett 287, 83–91. https://doi.org/10.1016/j.toxlet.2018.02.006.
[46] Useini, A., Engelberger, F., Künze, G., Sträter, N., 2023. Structural basis of the activation of PPARγ by the plasticizer metabolites MEHP and MINCH. Environ Int 173, 107822. https://doi.org/10.1016/j.envint.2023.107822.
[47] Langsch, A., David, R.M., Schneider, S., Sperber, S., Haake, V., Kamp, H., Leibold, E., Ravenzwaay, B. van, Otter, R., 2018. Hexamoll® DINCH: Lack of in vivo evidence for obesogenic properties. Toxicol Lett 288, 99–110. https://doi.org/10.1016/j.toxlet.2018.02.008.
[48] Krupka, S., Aldehoff, A.S., Goerdeler, C., Engelmann, B., Rolle-Kampczyk, U., Schubert, K., Klöting, N., von Bergen, M., Blüher, M., 2025. Metabolic and molecular Characterization, following dietary exposure to DINCH, Reveals new Implications for its role as a Metabolism-Disrupting chemical. Environ Int 196, 109306. https://doi.org/10.1016/j.envint.2025.109306.
[49] Braeuning, A., Balaguer, P., Bourguet, W., Carreras-Puigvert, J., Feiertag, K., Kamstra, J.H., Knapen, D., Lichtenstein, D., Marx-Stoelting, P., Rietdijk, J., Schubert, K., Spjuth, O., Stinckens, E., Thedieck, K., van den Boom, R., Vergauwen, L., von Bergen, M., Wewer, N., Zalko, D., 2023. Development of new approach methods for the identification and characterization of endocrine metabolic disruptors-a PARC project. Front Toxicol 5, 1212509. https://doi.org/10.3389/ftox.2023.1212509.
[50] Schmeisser, S., Miccoli, A., von Bergen, M., Berggren, E., Braeuning, A., Busch, W., Desaintes, C., Gourmelon, A., Grafström, R., Harrill, J., Hartung, T., Herzler, M., Kass, G.E.N., Kleinstreuer, N., Leist, M., Luijten, M., Marx-Stoelting, P., Poetz, O., van Ravenzwaay, B., Roggeband, R., Rogiers, V., Roth, A., Sanders, P., Thomas, R.S., Marie Vinggaard, A., Vinken, M., van de Water, B., Luch, A., Tralau, T., 2023. New approach methodologies in human regulatory toxicology - Not if, but how and when! Environ Int 178, 108082. https://doi.org/10.1016/j.envint.2023.108082.
[51] Pereira-Fernandes, A., Vanparys, C., Vergauwen, L., Knapen, D., Jorens, P.G., Blust, R., 2014. Toxicogenomics in the 3T3-L1 cell line, a new approach for screening of obesogenic compounds. Toxicol Sci 140, 352–363. https://doi.org/10.1093/toxsci/kfu092.
[52] Xu, T., Chen, L., Lim, Y.T., Zhao, H., Chen, H., Chen, M.W., Huan, T., Huang, Y., Sobota, R.M., Fang, M., 2021. System Biology-Guided Chemical Proteomics to Discover Protein Targets of Monoethylhexyl Phthalate in Regulating Cell Cycle. Environ Sci Technol 55, 1842–1851. https://doi.org/10.1021/acs.est.0c05832.
[53] Harrill, J.A., Viant, M.R., Yauk, C.L., Sachana, M., Gant, T.W., Auerbach, S.S., Beger, R.D., Bouhifd, M., O'Brien, J., Burgoon, L., Caiment, F., Carpi, D., Chen, T., Chorley, B.N., Colbourne, J., Corvi, R., Debrauwer, L., O'Donovan, C., Ebbels, T. M.D., Ekman, D.R., Faulhammer, F., Gribaldo, L., Hilton, G.M., Jones, S.P., Kende, A., Lawson, T.N., Leite, S.B., Leonards, P.E.G., Luijten, M., Martin, A., Moussa, L., Rudaz, S., Schmitz, O., Sobanski, T., Strauss, V., Vaccari, M., Vijay, V., Weber, R.J.M., Williams, A.J., Williams, A., Thomas, R.S., Whelan, M., 2021. Progress towards an OECD reporting framework for transcriptomics and metabolomics in regulatory toxicology. Regul Toxicol Pharm 125, 105020. https://doi.org/10.1016/j.yrtph.2021.105020.
[54] Franco, M.E., Fernandez-Luna, M.T., Ramirez, A.J., Lavado, R., 2020. Metabolomic-based assessment reveals dysregulation of lipid profiles in human liver cells exposed to environmental obesogens. Toxicol Appl Pharm 398, 115009. https://doi.org/10.1016/j.taap.2020.115009.
[55] Ramirez, T., Daneshian, M., Kamp, H., Bois, F.Y., Clench, M.R., Coen, M., Donley, B., Fischer, S.M., Ekman, D.R., Fabian, E., Guillou, C., Heuer, J., Hogberg, H.T., Jungnickel, H., Keun, H.C., Krennrich, G., Krupp, E., Luch, A., Noor, F., Peter, E., Riefke, B., Seymour, M., Skinner, N., Smirnova, L., Verheij, E., Wagner, S., Hartung, T., van Ravenzwaay, B., Leist, M., 2013. Metabolomics in toxicology and preclinical research. ALTEX 30, 209–225. https://doi.org/10.14573/altex.2013.2.209.
[56] Patti, G.J., Yanes, O., Siuzdak, G., 2012. Innovation: Metabolomics: the apogee of the omics trilogy. Nat Rev Mol Cell Biol 13, 263–269. https://doi.org/10.1038/nrm3314.
[57] Goerdeler, C., Engelmann, B., Aldehoff, A.S., Schaffert, A., Blüher, M., Heiker, J. T., Wabitsch, M., Schubert, K., Rolle-Kampczyk, U., von Bergen, M., 2024. Metabolomics in human SGBS cells as new approach method for studying adipogenic effects: Analysis of the effects of DINCH and MINCH on central carbon metabolism. Environ Res 252, 118847. https://doi.org/10.1016/j.envres.2024.118847.
[58] Jang, C., Chen, L., Rabinowitz, J.D., 2018. Metabolomics and Isotope Tracing. Cell 173, 822–837. https://doi.org/10.1016/j.cell.2018.03.055.
[59] Lauterbach, M.A., Hanke, J.E., Serefidou, M., Mangan, M.S.J., Kolbe, C.-C., Hess, T., Rothe, M., Kaiser, R., Hoss, F., Gehlen, J., Engels, G., Kreutzenbeck, M., Schmidt, S.V., Christ, A., Imhof, A., Hiller, K., Latz, E., 2019. Toll-like receptor signaling rewires macrophage metabolism and promotes histone acetylation via ATP-Citrate Lyase. Immunity 51, 997–1011.e7. https://doi.org/10.1016/j.immuni.2019.11.009.
[60] Morken, T.S., Brekke, E., Håberg, A., Widerøe, M., Brubakk, A.-M., Sonnewald, U., 2014. Neuron-astrocyte interactions, pyruvate carboxylation and the pentose phosphate pathway in the neonatal rat brain. Neurochem Res 39, 556–569. https://doi.org/10.1007/s11064-013-1014-3.
[61] Tews, D., Brenner, R.E., Siebert, R., Debatin, K.-M., Fischer-Posovszky, P., Wabitsch, M., 2022. 20 Years with SGBS cells - a versatile in vitro model of human adipocyte biology. Int J Obes 46, 1939–1947. https://doi.org/10.1038/s41366-022-01199-9.
[62] Axelsson, J., Rylander, L., Rignell-Hydbom, A., Jönsson, B.A.G., Lindh, C.H., Giwercman, A., 2015. Phthalate exposure and reproductive parameters in young men from the general Swedish population. Environ Int 85, 54–60. https://doi.org/10.1016/j.envint.2015.07.005.
[63] Huygh, J., Clotman, K., Malarvannan, G., Covaci, A., Schepens, T., Verbrugghe, W., Dirinck, E., van Gaal, L., Jorens, P.G., 2015. Considerable exposure to the endocrine disrupting chemicals phthalates and bisphenol-A in intensive care unit (ICU) patients. Environ Int 81, 64–72. https://doi.org/10.1016/j.envint.2015.04.008.
[64] Krycer, J.R., Quek, L.-E., Francis, D., Zadoorian, A., Weiss, F.C., Cooke, K.C., Nelson, M.E., Diaz-Vegas, A., Humphrey, S.J., Scalzo, R., Hirayama, A., Ikeda, S., Shoji, F., Suzuki, K., Huynh, K., Giles, C., Varney, B., Nagarajan, S.R., Hoy, A.J., Soga, T., Meikle, P.J., Cooney, G.J., Fazakerley, D.J., James, D.E., 2020. Insulin signaling requires glucose to promote lipid anabolism in adipocytes. J Biol Chem 295, 13250–13266. https://doi.org/10.1074/jbc.RA120.014907.
[65] Buescher, J.M., Moco, S., Sauer, U., Zamboni, N., 2010. Ultrahigh performance liquid chromatography-tandem mass spectrometry method for fast and robust quantification of anionic and aromatic metabolites. Anal Chem 82, 4403–4412. https://doi.org/10.1021/ac100101d.

[66] Heinrich, P., Kohler, C., Ellmann, L., Kuerner, P., Spang, R., Oefner, P.J., Dettmer, K., 2018. Correcting for natural isotope abundance and tracer impurity in MS-, MS/MS- and high-resolution-multiple-tracer-data from stable isotope labeling experiments with IsoCorrectoR. Sci Rep 8, 17910. https://doi.org/10.1038/s41598-018-36293-4.
[67] Oeckl, J., Bast-Habersbrunner, A., Fromme, T., Klingenspor, M., Li, Y., 2020. Isolation, culture, and functional analysis of murine thermogenic adipocytes. STAR Protoc 1, 100118. https://doi.org/10.1016/j.xpro.2020.100118.
[68] Felix, J.B., Cox, A.R., Hartig, S.M., 2021. Acetyl-CoA and metabolite fluxes regulate white adipose tissue expansion. Trends Endocrinol Metab 32, 320–332. https://doi.org/10.1016/j.tem.2021.02.008.
[69] Buescher, J.M., Antoniewicz, M.R., Boros, L.G., Burgess, S.C., Brunengraber, H., Clish, C.B., DeBerardinis, R.J., Feron, O., Frezza, C., Ghesquiere, B., Gottlieb, E., Hiller, K., Jones, R.G., Kamphorst, J.J., Kibbey, R.G., Kimmelman, A.C., Locasale, J.W., Lunt, S.Y., Maddocks, O.D.K., Malloy, C., Metallo, C.M., Meuillet, E.J., Munger, J., Nöh, K., Rabinowitz, J.D., Ralser, M., Sauer, U., Stephanopoulos, G., St-Pierre, J., Tennant, D.A., Wittmann, C., Vander Heiden, M. G., Vazquez, A., Vousden, K., Young, J.D., Zamboni, N., Fendt, S.-M., 2015. A roadmap for interpreting (13)C metabolite labeling patterns from cells. Curr Opin Biotechnol 34, 189–201. https://doi.org/10.1016/j.copbio.2015.02.003.
[70] Spalding, K.L., Arner, E., Westermark, P.O., Bernard, S., Buchholz, B.A., Bergmann, O., Blomqvist, L., Hoffstedt, J., Näslund, E., Britton, T., Concha, H., Hassan, M., Rydén, M., Frisén, J., Arner, P., 2008. Dynamics of fat cell turnover in humans. Nature 453, 783–787. https://doi.org/10.1038/nature06902.
[71] Lee, M.-J., Jash, S., Jones, J.E.C., Puri, V., Fried, S.K., 2019. Rosiglitazone remodels the lipid droplet and britens human visceral and subcutaneous adipocytes ex vivo. J Lipid Res 60, 856–868. https://doi.org/10.1194/jlr.M091173.
[72] Barquissau, V., Beuzelin, D., Pisani, D.F., Beranger, G.E., Mairal, A., Montagner, A., Roussel, B., Tavernier, G., Marques, M.-A., Moro, C., Guillou, H., Amri, E.-Z., Langin, D., 2016. White-to-brite conversion in human adipocytes promotes metabolic reprogramming towards fatty acid anabolic and catabolic pathways. Mol Metab 5, 352–365. https://doi.org/10.1016/j.molmet.2016.03.002.
[73] Halbgebauer, D., Dahlhaus, M., Wabitsch, M., Fischer-Posovszky, P., Tews, D., 2020. Browning capabilities of human primary adipose-derived stromal cells compared to SGBS cells. Sci Rep 10, 9632. https://doi.org/10.1038/s41598-020-64369-7.
[74] Klusóczki, Á., Veréb, Z., Vámos, A., Fischer-Posovszky, P., Wabitsch, M., Bacso, Z., Fésüs, L., Kristóf, E., 2019. Differentiating SGBS adipocytes respond to PPARγ stimulation, irisin and BMP7 by functional browning and beige characteristics. Sci Rep 9, 5823. https://doi.org/10.1038/s41598-019-42256-0.
[75] Shabalina, I.G., Petrovic, N., de Jong, J.M.A., Kalinovich, A.V., Cannon, B., Nedergaard, J., 2013. UCP1 in brite/beige adipose tissue mitochondria is functionally thermogenic. Cell Rep 5, 1196–1203. https://doi.org/10.1016/j.celrep.2013.10.044.
[76] McNally, K., Sams, C., Loizou, G., 2019. Development, testing, parameterization, and calibration of a human physiologically based pharmacokinetic model for the Plasticizer, Hexamoll® Diisononyl-Cyclohexane-1, 2-Dicarboxylate using in silico, in vitro, and human biomonitoring data. Front Pharm 10, 1394. https://doi.org/10.3389/fphar.2019.01394.
[77] Vrzáčková, N., Tomáško, J., Svoboda, P., Škop, V., Melčová, M., Dudová, J., Zelenka, J., Pulkrabová, J., Ruml, T., 2025. Accumulation of chlorinated paraffins in adipocytes is determined by cellular lipid content and chlorination level. Arch Toxicol 99, 1117–1131. https://doi.org/10.1007/s00204-024-03956-3.
[78] Dimitrijevic, D., Fabian, E., Nicol, B., Funk-Weyer, D., Landsiedel, R., 2022. Toward realistic dosimetry in vitro: determining effective concentrations of test substances in cell culture and their prediction by an in silico mass balance model. Chem Res Toxicol 35, 1962–1973. https://doi.org/10.1021/acs.chemrestox.2c00128.
[79] Aldehoff, A.S., Karkossa, I., Goerdeler, C., Krieg, L., Schor, J., Engelmann, B., Wabitsch, M., Landgraf, K., Hackermüller, J., Körner, A., Rolle-Kampczyk, U., Schubert, K., von Bergen, M., 2024. Unveiling the dynamics of acetylation and phosphorylation in SGBS and 3T3-L1 adipogenesis. iScience 27, 109711. https://doi.org/10.1016/j.isci.2024.109711.
[80] Kalkhof, S., Krieg, L., Büttner, P., Wabitsch, M., Küntzel, C., Friebe, D., Landgraf, K., Hanschkow, M., Schubert, K., Kiess, W., Krohn, K., Blüher, M., von Bergen, M., Körner, A., 2020. In Depth Quantitative Proteomic and Transcriptomic Characterization of Human Adipocyte Differentiation Using the SGBS Cell Line. Proteomics, e1900405. https://doi.org/10.1002/pmic.201900405.
[81] Proença, S., Escher, B.I., Fischer, F.C., Fisher, C., Grégoire, S., Hewitt, N.J., Nicol, B., Paini, A., Kramer, N.I., 2021. Effective exposure of chemicals in in vitro cell systems: A review of chemical distribution models. Toxicol Vitr 73, 105133. https://doi.org/10.1016/j.tiv.2021.105133.
[82] Oates, E.H., Antoniewicz, M.R., 2022. Coordinated reprogramming of metabolism and cell function in adipocytes from proliferation to differentiation. Metab Eng 69, 221–230. https://doi.org/10.1016/j.ymben.2021.12.005.
[83] Liu, L., Shah, S., Fan, J., Park, J.O., Wellen, K.E., Rabinowitz, J.D., 2016. Malic enzyme tracers reveal hypoxia-induced switch in adipocyte NADPH pathway usage. Nat Chem Biol 12, 345–352. https://doi.org/10.1038/nchembio.2047.
[84] Si, Y., Shi, H., Lee, K., 2009. Impact of perturbed pyruvate metabolism on adipocyte triglyceride accumulation. Metab Eng 11, 382–390. https://doi.org/10.1016/j.ymben.2009.08.001.
[85] Santoro, A., McGraw, T.E., Kahn, B.B., 2021. Insulin action in adipocytes, adipose remodeling, and systemic effects. Cell Metab 33, 748–757. https://doi.org/10.1016/j.cmet.2021.03.019.
[86] Vergnes, L., Chin, R., Young, S.G., Reue, K., 2011. Heart-type fatty acid-binding protein is essential for efficient brown adipose tissue fatty acid oxidation and cold tolerance. J Biol Chem 286, 380–390. https://doi.org/10.1074/jbc.M110.184754.
[87] Bauzá-Thorbrügge, M., Vujičić, M., Chanclón, B., Palsdottir, V., Pillon, N.J., Benrick, A., Wernstedt Asterholm, I., 2024. Adiponectin stimulates Sca1+CD34– adipocyte precursor cells associated with hyperplastic expansion and beiging of brown and white adipose tissue. Metab Clin Exp 151, 155716. https://doi.org/10.1016/j.metabol.2023.155716.
[88] Inagaki, T., Sakai, J., Kajimura, S., 2016. Transcriptional and epigenetic control of brown and beige adipose cell fate and function. Nat Rev Mol Cell Biol 17, 480–495. https://doi.org/10.1038/nrm.2016.62.
[89] Miller, C.N., Yang, J.-Y., England, E., Yin, A., Baile, C.A., Rayalam, S., 2015. Isoproterenol Increases Uncoupling, Glycolysis, and Markers of Beiging in Mature 3T3-L1 Adipocytes. PLOS ONE 10, e0138344. https://doi.org/10.1371/journal.pone.0138344.
[90] Reshef, L., Olswang, Y., Cassuto, H., Blum, B., Croniger, C.M., Kalhan, S.C., Tilghman, S.M., Hanson, R.W., 2003. Glyceroneogenesis and the triglyceride/fatty acid cycle. J Biol Chem 278, 30413–30416. https://doi.org/10.1074/jbc.R300017200.
[91] Mills, E.L., Pierce, K.A., Jedrychowski, M.P., Garrity, R., Winther, S., Vidoni, S., Yoneshiro, T., Spinelli, J.B., Lu, G.Z., Kazak, L., Banks, A.S., Haigis, M.C., Kajimura, S., Murphy, M.P., Gygi, S.P., Clish, C.B., Chouchani, E.T., 2018. Accumulation of succinate controls activation of adipose tissue thermogenesis. Nature 560, 102–106. https://doi.org/10.1038/s41586-018-0353-2.
[92] Cannon, B., Nedergaard, J., 1979. The physiological role of pyruvate carboxylation in hamster brown adipose tissue. Eur J Biochem 94, 419–426. https://doi.org/10.1111/j.1432-1033.1979.tb12909.x.
[93] Yang, C., Ko, B., Hensley, C.T., Jiang, L., Wasti, A.T., Kim, J., Sudderth, J., Calvaruso, M.A., Lumata, L., Mitsche, M., Rutter, J., Merritt, M.E., DeBerardinis, R.J., 2014. Glutamine oxidation maintains the TCA cycle and cell survival during impaired mitochondrial pyruvate transport. Mol Cell 56, 414–424. https://doi.org/10.1016/j.molcel.2014.09.025.
[94] Sharma, A.K., Khandelwal, R., Wolfrum, C., 2024. Futile lipid cycling: from biochemistry to physiology. Nat Metab 6, 808–824. https://doi.org/10.1038/s42255-024-01003-0.
[95] Chubukov, V., Uhr, M., Le Chat, L., Kleijn, R.J., Jules, M., Link, H., Aymerich, S., Stelling, J., Sauer, U., 2013. Transcriptional regulation is insufficient to explain substrate-induced flux changes in Bacillus subtilis. Mol Syst Biol 9, 709. https://doi.org/10.1038/msb.2013.66.
[96] Ralser, M., Wamelink, M.M.C., Latkolik, S., Jansen, E.E.W., Lehrach, H., Jakobs, C., 2009. Metabolic reconfiguration precedes transcriptional regulation in the antioxidant response. Nat Biotechnol 27, 604–605. https://doi.org/10.1038/nbt0709-604.
[97] Li, Y., Wang, D., Ping, X., Zhang, Y., Zhang, T., Wang, L., Jin, L., Zhao, W., Guo, M., Shen, F., Meng, M., Chen, X., Zheng, Y., Wang, J., Li, D., Zhang, Q., Hu, C., Xu, L., Ma, X., 2022. Local hyperthermia therapy induces browning of white fat and treats obesity, 949-966.e19 Cell 185. https://doi.org/10.1016/j.cell.2022.02.004.
[98] Cheng, C.-F., Ku, H.-C., Cheng, J.-J., Chao, S.-W., Li, H.-F., Lai, P.-F., Chang, C.-C., Don, M.-J., Chen, H.-H., Lin, H., 2019. Adipocyte browning and resistance to obesity in mice is induced by expression of ATF3. Commun Biol 2, 389. https://doi.org/10.1038/s42003-019-0624-y.
[99] Petruzzelli, M., Schweiger, M., Schreiber, R., Campos-Olivas, R., Tsoli, M., Allen, J., Swarbrick, M., Rose-John, S., Rincon, M., Robertson, G., Zechner, R., Wagner, E.F., 2014. A switch from white to brown fat increases energy expenditure in cancer-associated cachexia. Cell Metab 20, 433–447. https://doi.org/10.1016/j.cmet.2014.06.011.
[100] Abdullahi, A., Samadi, O., Auger, C., Kanagalingam, T., Boehning, D., Bi, S., Jeschke, M.G., 2019. Browning of white adipose tissue after a burn injury promotes hepatic steatosis and dysfunction. Cell Death Dis 10, 870. https://doi.org/10.1038/s41419-019-2103-2.
[101] Nemetchek, M.D., Chrisman, I.M., Rayl, M.L., Voss, A.H., Hughes, T.S., 2022. A structural mechanism of nuclear receptor biased agonism. Proc Natl Acad Sci USA 119, e2215333119. https://doi.org/10.1073/pnas.2215333119.
[102] Aldehoff, A.S., Karkossa, I., Broghammer, H., Krupka, S., Weiner, J., Goerdeler, C., Nuwayhid, R., Langer, S., Wabitsch, M., Rolle-Kampczyk, U., Klöting, N., Blüher, M., Heiker, J.T., von Bergen, M., Schubert, K., 2025. Advanced Proteomics Approaches Hold Potential for the Risk Assessment of Metabolism-Disrupting Chemicals as Omics-Based NAM: A Case Study Using the Phthalate Substitute DINCH. Environ Sci Technol. https://doi.org/10.1021/acs.est.5c01206.
[103] Yang, W., Zheng, Y., Xia, Y., Ji, H., Chen, X., Guo, F., Lyssiotis, C.A., Aldape, K., Cantley, L.C., Lu, Z., 2012. ERK1/2-dependent phosphorylation and nuclear translocation of PKM2 promotes the Warburg effect. Nat Cell Biol 14, 1295–1304. https://doi.org/10.1038/ncb2629.
[104] Ma, H., Zhang, J., Zhou, L., Wen, S., Tang, H.-Y., Jiang, B., Zhang, F., Suleman, M., Sun, D., Chen, A., Zhao, W., Lin, F., Tsau, M.-T., Shih, L.-M., Xie, C., Li, X., Lin, D., Hung, L.-M., Cheng, M.-L., Li, Q., 2020. c-Src Promotes Tumorigenesis and Tumor Progression by Activating PFKFB3. Cell Rep 30, 4235–4249.e6. https://doi.org/10.1016/j.celrep.2020.03.005.
[105] Domínguez-Romero, E., Komprdová, K., Kalina, J., Bessems, J., Karakitsios, S., Sarigiannis, D.A., Scheringer, M., 2023. Time-trends in human urinary

concentrations of phthalates and substitutes DEHT and DINCH in Asian and North American countries (2009-2019). J Expo Sci Environ Epidemiol 33, 244–254. https://doi.org/10.1038/s41370-022-00441-w.

[106] Bhat, V.S., Durham, J.L., Ball, G.L., English, J.C., 2014. Derivation of an oral reference dose (RfD) for the nonphthalate alternative plasticizer 1,2-cyclohexane dicarboxylic acid, di-isononyl ester (DINCH). J Toxicol Environ Health Part B 17, 63–94. https://doi.org/10.1080/10937404.2013.876288.

[107] Bérubé, R., LeFauve, M.K., Heldman, S., Chiang, Y.-T.T., Birbeck, J., Westrick, J., Hoffman, K., Kassotis, C.D., 2023. Adipogenic and endocrine disrupting mixture effects of organic and inorganic pollutant mixtures. Sci Total Environ 876, 162587. https://doi.org/10.1016/j.scitotenv.2023.162587.

[108] Philippat, C., Rolland, M., Lyon-Caen, S., Pin, I., Sakhi, A.K., Sabaredzovic, A., Thomsen, C., Slama, R., 2021. Pre- and early post-natal exposure to phthalates and DINCH in a new type of mother-child cohort relying on within-subject pools of repeated urine samples. Environ Pollut 287, 117650. https://doi.org/10.1016/j.envpol.2021.117650.

[109] Geserick, M., Vogel, M., Gausche, R., Lipek, T., Spielau, U., Keller, E., Pfäffle, R., Kiess, W., Körner, A., 2018. Acceleration of BMI in Early Childhood and Risk of Sustained Obesity. N Engl J Med 379, 1303–1312. https://doi.org/10.1056/NEJMoa1803527.

[110] Arner, P., Rydén, M., 2022. Human white adipose tissue: A highly dynamic metabolic organ. J Intern Med 291, 611–621. https://doi.org/10.1111/joim.13435.

[111] Pereira-Fernandes, A., Demaegdt, H., Vandermeiren, K., Hectors, T.L.M., Jorens, P.G., Blust, R., Vanparys, C., 2013. Evaluation of a screening system for obesogenic compounds: screening of endocrine disrupting compounds and evaluation of the PPAR dependency of the effect. PLOS ONE 8, e77481. https://doi.org/10.1371/journal.pone.0077481.

[112] Kim, S., Reed, E., Monti, S., Schlezinger, J.J., 2021. A data-driven transcriptional taxonomy of adipogenic chemicals to identify white and brite adipogens. Environ Health Persp 129, 77006. https://doi.org/10.1289/EHP6886.

[113] Modaresi, S.M.S., Wei, W., Emily, M., DaSilva, N.A., Slitt, A.L., 2022. Per- and polyfluoroalkyl substances (PFAS) augment adipogenesis and shift the proteome in murine 3T3-L1 adipocytes. Toxicology 465, 153044. https://doi.org/10.1016/j.tox.2021.153044.

[114] Schwender, J., König, C., Klapperstück, M., Heinzel, N., Munz, E., Hebbelmann, I., Hay, J.O., Denolf, P., de Bodt, S., Redestig, H., Caestecker, E., Jakob, P.M., Borisjuk, L., Rolletschek, H., 2014. Transcript abundance on its own cannot be used to infer fluxes in central metabolism. Front Plant Sci 5, 668. https://doi.org/10.3389/fpls.2014.00668.

[115] Sud, M., Fahy, E., Cotter, D., Azam, K., Vadivelu, I., Burant, C., Edison, A., Fiehn, O., Higashi, R., Nair, K.S., Sumner, S., Subramaniam, S., 2016. Metabolomics Workbench: An international repository for metabolomics data and metadata, metabolite standards, protocols, tutorials and training, and analysis tools. Nucleic Acids Res 44, D463–D470. https://doi.org/10.1093/nar/gkv1042.